

Scaling properties of invariant densities of coupled Tchebyscheff maps

Stefan Groote^{1,2} and Christian Beck³

¹ Institut für Physik der Johannes-Gutenberg-Universität,
Staudinger Weg 7, 55099 Mainz, Germany

² Füüsika-Keemiateaduskond, Tartu Ülikool, Tähe 4, 51010 Tartu, Estonia

³ School of Mathematical Sciences, Queen Mary,
University of London, Mile End Road, London E1 4NS, UK

Abstract

We study 1-dimensional coupled map lattices consisting of diffusively coupled Tchebyscheff maps of N -th order. For small coupling constants a we determine the invariant 1-point and 2-point densities of these nonhyperbolic systems in a perturbative way. For arbitrarily small couplings $a > 0$ the densities exhibit a selfsimilar cascade of patterns, which we analyse in detail. We prove that there are log-periodic oscillations of the density both in phase space as well as in parameter space. We show that expectations of arbitrary observables scale with \sqrt{a} in the low-coupling limit, contrasting the case of hyperbolic maps where one has scaling with a . Moreover we prove that there are log-periodic oscillations of period $\log N^2$ modulating the \sqrt{a} -dependence of the expectation value of any given observable.

1 Introduction

Coupled map lattices (CMLs) as introduced by Kaneko and Kapral [1, 2] are interesting examples of spatially extended dynamical systems that exhibit a rich structure of complex dynamical phenomena [3, 4, 5, 6, 7]. Both space and time are discrete for these types of dynamical systems, but the local field variable at each lattice site takes on continuous values. CMLs have a variety of applications: They have been studied e.g. as models for hydrodynamical flows, turbulence, chemical reactions, biological systems, and quantum field theories (see e.g. reviews in [3, 4]). Of particular interest are CMLs that exhibit spatio-temporal chaotic behaviour. The analysis of these types of CMLs is often restricted to numerical investigations and only a few analytical results are known. A notable exception is the case of CMLs consisting locally of hyperbolic maps for small coupling a . Here a variety of analytical results is known [8, 9, 10, 11] that guarantee the existence of a smooth invariant density and ergodic behaviour.

The situation is much more complicated for nonhyperbolic local maps which correspond to the generic case of physical interest [12, 13, 14, 15, 16, 17]. In the one-dimensional case, non-hyperbolicity simply means that the absolute value of the slope of the local map is allowed to be smaller than 1 in some regions. For chaotic CMLs consisting of nonhyperbolic maps much less is known analytically, and standard techniques from ergodic theory are usually not applicable. From the applications point of view, the nonhyperbolic case is certainly the most interesting one. For example, it has been shown that nonhyperbolic CMLs exhibiting spatio-temporal chaos naturally arise from stochastically quantised scalar field theories in a suitable limit where the strength of the underlying self-interacting potentials goes to infinity [4, 18]. CMLs obtained in this way can serve as useful models for vacuum fluctuations and dark energy in the universe [19]. Other applications include chemical kinetics as described by discretised reaction diffusion dynamics [3].

In this paper, we study weakly coupled N -th order Tchebyscheff maps [17, 18, 19, 20, 21, 22]. We consider CMLs with diffusive coupling, i.e. there is a coupling between neighboured maps that resembles a discrete version of the Laplacian on the lattice. This form of the coupling is the most important one for the quantum field theoretical applications [4]. In the uncoupled case it is well known that the Tchebyscheff maps are conjugated to a Bernoulli shift of N symbols (see, e.g. [23]). In the coupled case, this conjugacy is destroyed and the conventional treatments for hyperbolic maps does not apply, since the Tchebyscheff maps have $N - 1$ critical points where the slope vanishes, thus corresponding to a nonhyperbolic situation.

We will derive explicit formulas for the invariant densities describing the ergodic behaviour of weakly coupled Tchebyscheff systems, by applying a perturbative treatment. Our analytical techniques will yield explicit perturbative expressions for the invariant 1-point and 2-point density for small couplings a . We will prove a variety of interesting results concerning the scaling behaviour of these nonhyperbolic systems. Our main results are that the 1-point density exhibits log-periodic oscillations of period $\log N^2$ near the edges of the interval. Expectations of typical observables scale with \sqrt{a} (rather than with a as for hyperbolic coupled maps). We also show that there are log-periodic modulations of arbitrary expectation values as a function of the coupling parameter a . Although our results are rigorously derived for the explicit example of Tchebyscheff maps only, we expect that similar results hold for other nonhyperbolic systems as well, since our techniques are quite general and can be applied to various other systems in a similar way.

This paper is organized as follows: In section 2 we introduce the relevant class of coupled map lattices and provide some numerical evidence for the observed scaling phenomena, choosing as a main example the Ulam map (the $N = 2$ Tchebyscheff map). Our perturbative theory of the invariant density of the coupled system is presented in section 3. Based on these results we explain details of the selfsimilar patterns in section 4. In section 5 we extend our results to the third order Tchebyscheff map, where, due to an additional discrete symmetry, the behaviour is somewhat different as compared to $N = 2$. Finally, in section 6 we collect our results to finally prove that there are log-periodic oscillations modulating the scaling behaviour of expectation values of arbitrary observables if the coupling parameter a is changed.

2 Observed scaling phenomena

We consider one-dimensional coupled map lattices of the form

$$\phi_{n+1}^i = (1 - a)T_N(\phi_n^i) + s\frac{a}{2} \left(T_N^b(\phi_n^{i-1}) + T_N^b(\phi_n^{i+1}) \right). \quad (1)$$

Here $T_N(\phi)$ denotes the N -th order Tchebyscheff polynomial and ϕ_n^i is a local iterate at lattice site i at time n . Our main interest is concentrated on the cases $N = 2$ where $T_2(\phi) = 2\phi^2 - 1$ and $N = 3$ where $T_3(\phi) = 4\phi^3 - 3\phi$. The sign $s = \pm 1$ distinguishes between the ‘diffusive coupling’ ($s = +1$) and the ‘anti-diffusive coupling’ ($s = -1$). The index b finally can take the values $b = 0, 1$ where $b = 1$ corresponds to forward coupling ($T_N^1(\phi) := T_N(\phi)$) whereas $b = 0$ stands for backward coupling ($T_N^0(\phi) := \phi$). The discrete chaotic noise field variables ϕ_n^i take on continuous values on the interval $[-1, 1]$. The initial values ϕ_0^i are randomly chosen in this interval with a smooth density, usually chosen to be the invariant density of the uncoupled system.

2.1 Scaling in parameter space

The variable a in Eq. (1) is a coupling parameter which takes values in the interval $[0, 1]$. It determines the strength of the Laplacian coupling in Eq. (1) (in the particle physics applications described in [4] a^{-1} can be regarded as a kind of metric for a one-dimensional ‘chaotic string’). For $a = 0$ we end up with the chaotic behaviour $\phi_{n+1}^i = T_N(\phi_n^i)$ as generated by uncoupled Tchebyscheff maps. If a small coupling $a > 0$ is switched on, one observes the formation of nontrivial density patterns with scaling behaviour with respect to \sqrt{a} . Consider an arbitrary test function (observable) $V(\phi)$ of the local iterates, and let $\langle \dots \rangle_a$ denote the expectation values formed by long-term iteration and averaging over all lattice sites. For small a one observes numerically

$$\langle V(\phi) \rangle_a - \langle V(\phi) \rangle_0 = f^{(N)}(\ln a) a^{1/2} \quad (2)$$

where $f^{(N)}(\ln a)$ is a periodic function of $\ln a$ with period $\ln N^2$. The function $f^{(N)} = f^{(N)}[V]$ is a functional of V . A double logarithmic plot of $|\langle V(\phi) \rangle_a - \langle V(\phi) \rangle_0|$ versus a hence shows a straight line that is modulated by oscillating behaviour. Examples are shown in Fig. 1. We will rigorously prove the observed log-periodic scaling behaviour with respect to a in section 6 of this paper.

For small a there is no difference between expectations calculated with the forward or backward coupling form of (1), the value of b matters only for large values of the coupling.

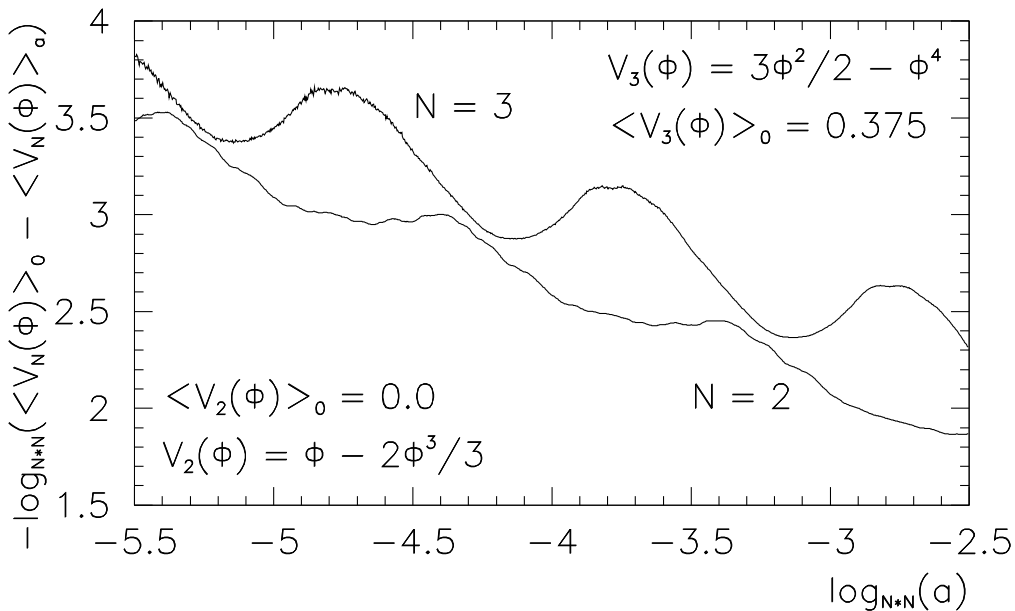


Figure 1: Scaling in parameter space for the test functions $V(\phi) = V_2(\phi) := \phi - \frac{2}{3}\phi^3$ ($N = 2$) and $V(\phi) = V_3(\phi) := \frac{3}{2}\phi^2 - \phi^4$ ($N = 3$)

2.2 Scaling in the phase space

There is also scaling behaviour in the phase space of the coupled system. First, let us consider the uncoupled case. The invariant (one-point probability) density corresponding to $a = 0$ is known to be

$$\rho_0(\phi) = \frac{1}{\pi\sqrt{1-\phi^2}} \quad (3)$$

(see e.g. [23] for a derivation). This density is universal in the sense that it does not depend on the index N of the Tchebyscheff polynomial for $N \geq 2$.

The 1-point invariant density at each lattice site will of course change if we consider values $a \neq 0$. It then depends not only on a but also on the index N . In other words, the N -degeneracy is broken for finite coupling. In principle, the invariant densities of coupled map lattices can be understood by finding fixed points of the Perron-Frobenius operator of these very high-dimensional dynamical systems [10, 24, 25, 26, 27]. The 1-point density can then be obtained as a marginal distribution, by integrating out all lattice degrees of freedom up to one. In practice, this program is rather complicated for our type of systems and we will apply a more pedestrian but feasible method in the following sections.

If the coupling a is slightly increased starting from $a = 0$, the invariant 1-point density $\rho_a(\phi)$ starts to deviate from $\rho_0(\phi)$. There are particularly strong deviations at the boundaries $\phi = \pm 1$ of the interval. While for odd N the evolution equation (1) is invariant under the replacement $\phi \rightarrow -\phi$ and hence the invariant density is symmetric, this is not the case for even values of N . In both cases we are interested in the region close to $\phi = \pm 1$ and our goal is to understand the deviation of $\rho_a(\phi)$ from $\rho_0(\phi)$.

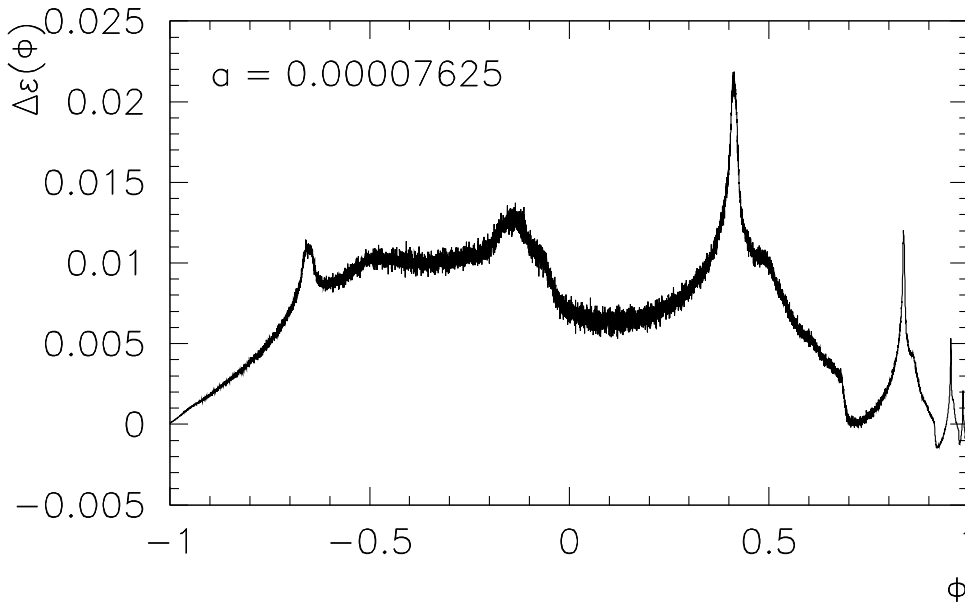


Figure 2: Energy difference $\Delta\epsilon(\phi)$ for the 2B-string at $a = 0.00007625$

For our purpose it is useful to define an ‘effective energy’ ϵ_a as follows:

$$\epsilon_a(\phi) := \frac{1}{2} - \frac{1}{2\pi^2 \rho_a(\phi)^2}. \quad (4)$$

For $a = 0$ this effective energy is just given by the ‘kinetic energy’ expression $\frac{1}{2}\phi^2$ of a free particle, and the invariant density coincides with that of a generalized canonical ensemble in Tsallis’ formulation of nonextensive statistical mechanics [28], the entropic index q being given by $q = 3$. For $a \neq 0$ the effective energy becomes more complicated and it includes the effects of interactions with neighbored lattice sites. The quantity of interest is the energy difference $\Delta\epsilon(\phi) = \epsilon_a(\phi) - \epsilon_0(\phi)$.

In [4] a general classification scheme of the relevant Tchebyscheff CMLs was introduced. To be specific, let us here consider the coupled Tchebyscheff map system with $N = 2$, $s = +1$ and $b = 0$ (called 2B-string in [4]). For finite a we obtain an (asymmetric) energy difference $\Delta\epsilon(\phi)$ which when approaching the boundary $\phi = +1$ shows selfsimilar behaviour, i.e. a repetition of nearly the same pattern if a suitable rescaling is done (see Fig. 2).

The scaling behaviour close to $\phi = +1$ can be analysed in more detail by looking at a logarithmic plot of $\Delta\epsilon(\phi)$ versus $\phi^* = -\log_4(1 - \phi)$, as shown in Fig. 3. In order to deal with a logarithmic histogram plot the data are adjusted in the usual way by the factor $1/(1 - \phi) \ln 4$, as obtained from transformation of random variables. We see that the pattern in this plot is repeated with a period $\Delta\phi^* = 1$, though there is a sharp breakdown of periodicity at the value $\phi^* = a^* = -\log_4(4a)$. We will prove this behaviour later.

2.3 Connection between parameter and phase space scaling

Let us now look at how the energy difference changes with the coupling parameter a . If the coupling is decreased by a factor of 4 one observes that the pattern in the logarithmic plot is

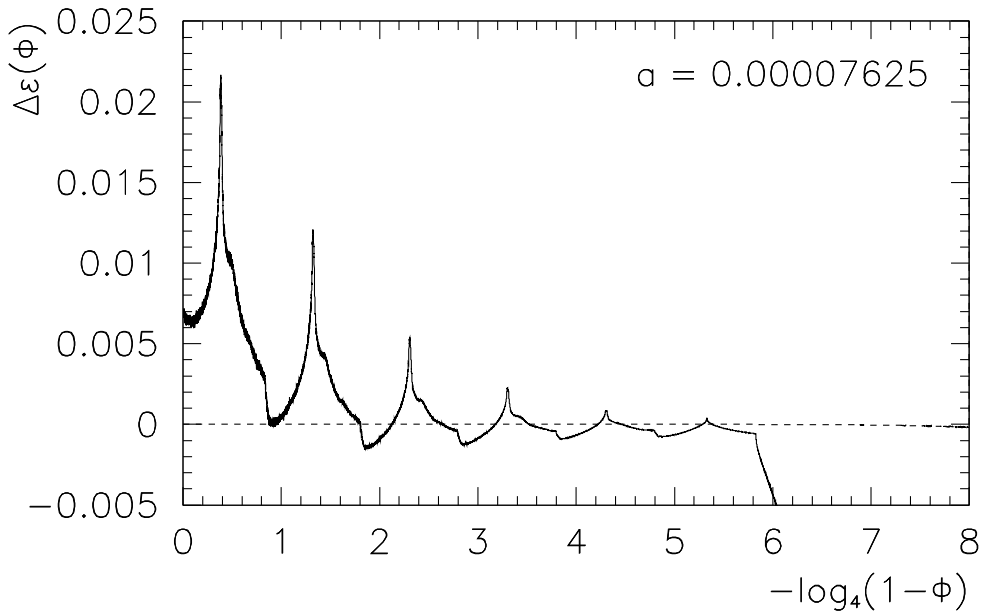


Figure 3: Energy difference $\Delta\epsilon(\phi)$ for the 2B-string for $a = 0.00007625$ (logarithmic plot)

moved to the right by $\Delta\phi^* = 1$ while a new pattern element is created to the left. The picture is like a wave generator located at $\phi^* = 0$ that was started at some ‘time’ in the past and is sending out waves with a speed $\Delta\phi^* = 1$. In this analogy ‘time’ corresponds to the negative logarithm of the coupling parameter. Since in Fig. 3 the pattern amplitude becomes smaller and smaller towards higher values of ϕ^* we can try to compensate this effect by multiplying $\Delta\epsilon(\phi)$ by an appropriate simple function of ϕ^* . It turns out that the multiplication by $\rho_0(\phi)$ compensates the decrease of the pattern for a fixed value of the coupling a . However, the pattern as a whole turns out to decrease by a factor of 2 if we divide the coupling by a factor of 4. Therefore, as a last adjustment, we multiply with the inverse square root $1/\sqrt{a}$ of the coupling. In a sequence of steps $\Delta a^* = 1$ for the ‘time variable’ $a^* = -\log_4(4a)$ we show in Fig. 4 the progressive motion of the adjusted pattern, indicating the breakdown point at $\phi^* = a^*$.

We can compensate the shift of the pattern to the right by subtracting $a^* = -\log_4(4a)$ from $\phi^* = -\log_4(1-\phi)$ obtaining the new variable $x^* = \phi^* - a^*$. Note that x^* is negative beyond the breakdown region. In writing subsequent curves into the same diagram we obtain an entire set of curves shown in Fig. 5. While the curves diverge for large absolute values of x^* , the surprising fact is that they exactly coincide close to the breakdown at $x^* = 0$. This means that there is invariance under a suitable renormalization transformation: $a^{-1/2}\rho_0(\phi)\Delta\epsilon(\phi)$ is a function of $x^* = -\log_4(x)$ only if the absolute value of x^* is small. The shape of the first peak (i.e. for $x^* \in [-1, 0]$) seems to be very simple, while the following peaks increase in complexity.

As a last diagram illustrating this behaviour, in Fig. 6 we show the development of the density pattern for a given fixed interval of ϕ^* for the already used sequence of values of a . Note the slight shift of the maxima to the left and the formation of plateaus. Various details of this figure will become clearer by our theoretical treatment in section 4.

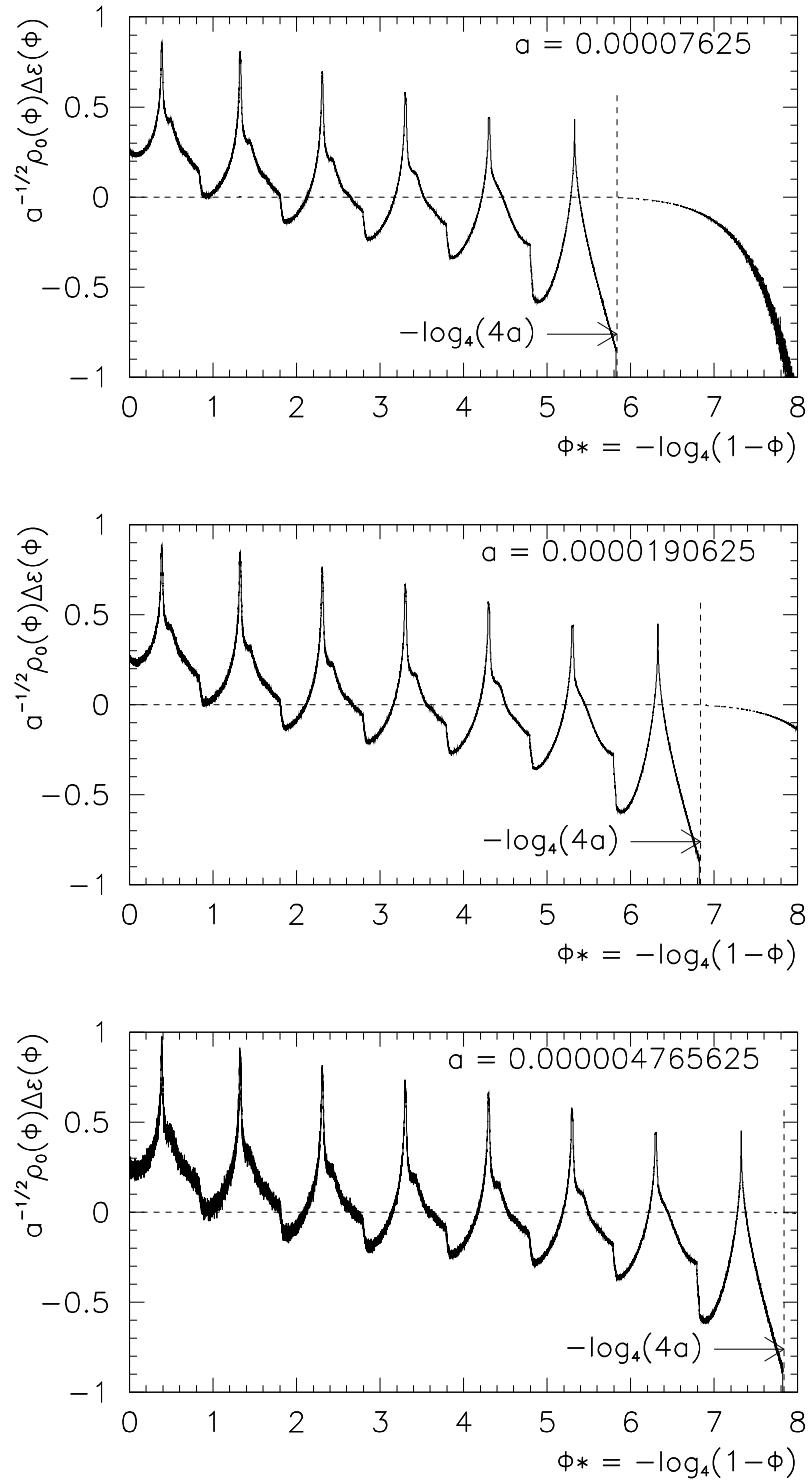


Figure 4: Adjusted energy difference $a^{-1/2} \rho_0(\phi) \Delta \epsilon(\phi)$ for the 2B-string at $a = 0.00007625$, $a = 0.0000190625$, and $a = 0.000004765625$ (from top to bottom). Indicated is the breakdown point of the pattern at $\phi^* = a^* = -\log_4(4a)$ (vertical line) as well as the pattern amplitude multiplied by a factor of 0.001 (horizontal line) in order to have a suitable scale for the breakdown region

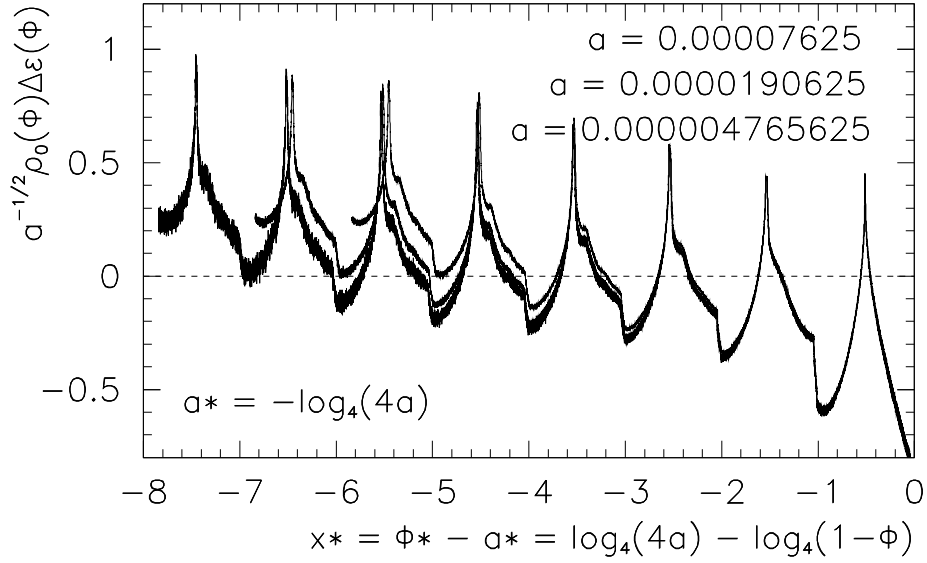


Figure 5: Adjusted energy difference $a^{-1/2}\rho_0(\phi)\Delta\epsilon(\phi)$ for the 2B-string at $a = 0.00007625$, $a = 0.0000190625$, and $a = 0.000004765625$ (from top to bottom) as a function of $x^* = \phi^* - a^*$.

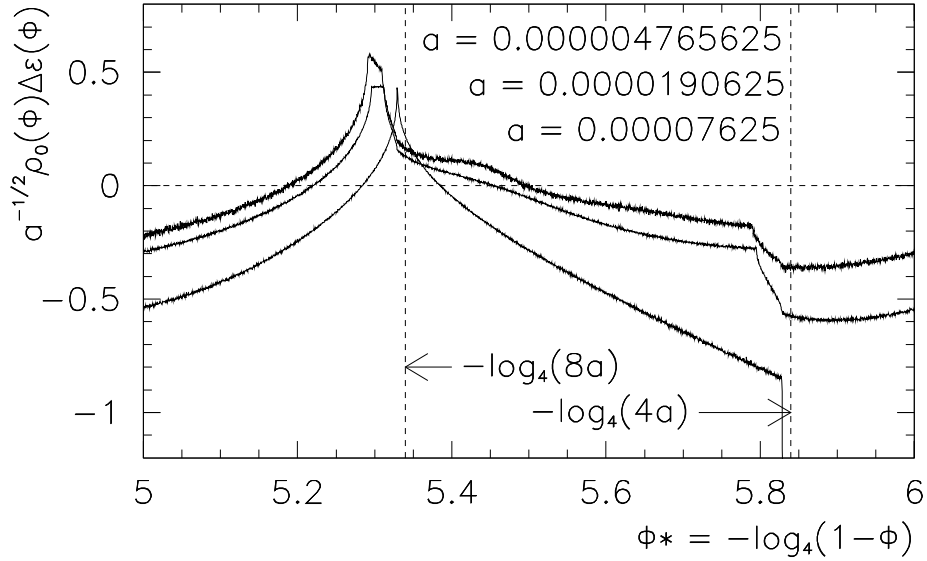


Figure 6: Comparison of the first three peaks, as obtained for a fixed interval of ϕ^* with $a = 0.00007625$, $a = 0.0000190625$, and $a = 0.000004765625$. The indicated logarithms in the diagram are related to the value $a = 0.00007625$.

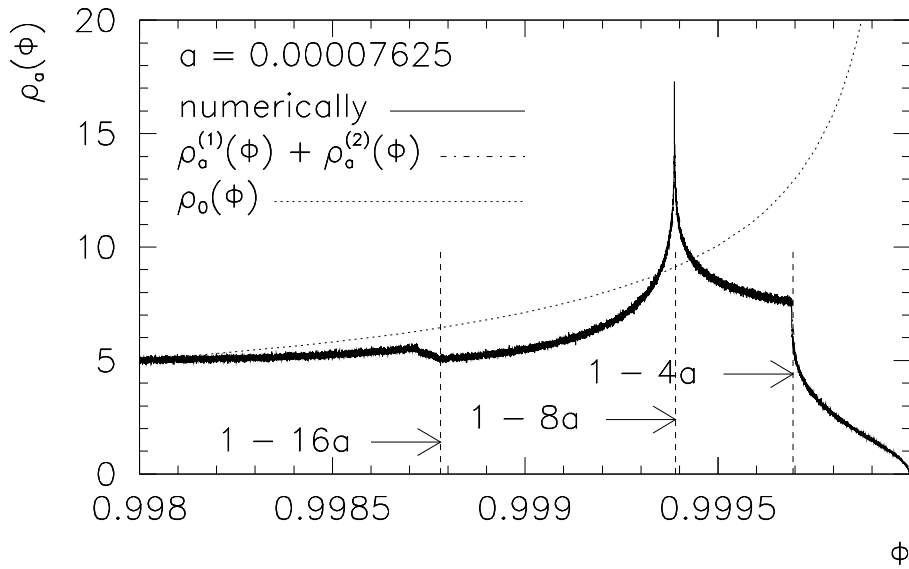


Figure 7: Invariant density $\rho_a(\phi)$ close to $\phi = +1$ for the 2B-string for $a=0.00007625$, as compared to the invariant density $\rho_0(\phi)$ for vanishing coupling (dotted curve).

3 Perturbative calculation of the invariant density

Let us now proceed to an analytic (perturbative) calculation of the invariant 1-point density of the 2B-dynamics

$$\phi_{n+1}^i = (1-a)T_2(\phi_n^i) + \frac{a}{2}(\phi_n^{i-1} + \phi_n^{i+1}). \quad (5)$$

We are particularly interested in the behaviour near the boundaries $\phi = \pm 1$. The numerically determined density near $\phi = +1$ is shown in Fig. 7.

As a first approximation, we essentially regard the system (5) as a perturbed one-dimensional system, the perturbation of strength a given by the arithmetic mean of nearest neighbours $(\phi_n^{i-1} + \phi_n^{i+1})/2 =: (\phi_+ + \phi_-)/2 =: \tilde{\phi}$. As a first approximation we may also regard ϕ_+ and ϕ_- to be nearly independent for small a , provided we are not too close to the edges of the interval. The probability density ρ_{aa} of $\tilde{\phi}$ is obtained by the convolution

$$\rho_{aa}(\tilde{\phi}) = 2 \int \rho_a(2\tilde{\phi} - \phi_-)\rho_a(\phi_-)d\phi_-, \quad (6)$$

the factor 2 arising from the fact that $d\phi_+d\phi_- = 2d\tilde{\phi}d\phi_-$. If we replace the densities ρ_a occurring in Eq. (6) by ρ_0 , we can calculate the convolution analytically to obtain

$$\rho_{00}(\tilde{\phi}) = \int \frac{2d\phi_-}{\pi^2 \sqrt{1 - (2\tilde{\phi} - \phi_-)^2} \sqrt{1 - \phi_-^2}} = \frac{2}{\pi^2} K\left(\sqrt{1 - \tilde{\phi}^2}\right) \theta(1 - \tilde{\phi}^2), \quad (7)$$

where $K(x)$ is the complete elliptic integral of the first kind. The functions $\rho_0(\phi)$ and $\rho_{00}(\phi)$ are shown in Fig. 8. If we calculate to leading order, we can always replace $\rho_a(\phi)$ and $\rho_{aa}(\phi)$ by $\rho_0(\phi)$ and $\rho_{00}(\phi)$, respectively.

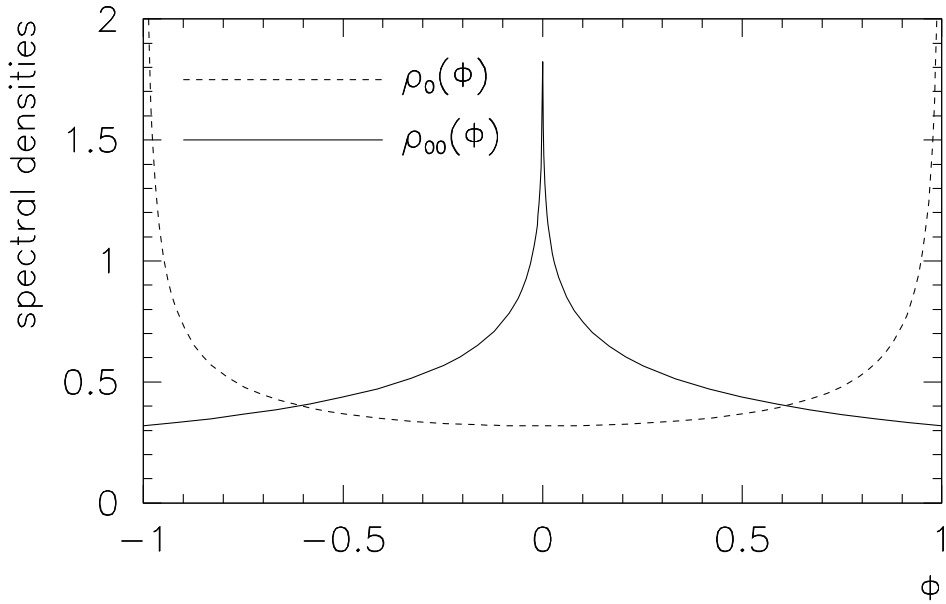


Figure 8: Invariant densities $\rho_{00}(\phi)$ (solid line) and $\rho_0(\phi)$ (dashed line)

3.1 The zeroth iterate of the convolution formula

Having the density $\rho_{aa}(\tilde{\phi})$ at hand, we can now calculate the probability that the value ϕ in an interval of length $d\phi$ and the value $\tilde{\phi}$ in an interval of length $d\tilde{\phi}$ give rise to a value $\phi' = (1-a)T_2(\phi) + a\tilde{\phi}$ in an interval of length $d\phi'$,

$$\rho_a(\phi') = \frac{1}{a} \rho_a(\phi) \rho_{aa}((\phi' - (1-a)T_2(\phi))/a) d\phi. \quad (8)$$

Note that there is an implicit constraint in this equation that restricts the integration range of ϕ , given by the condition $|\tilde{\phi}| \leq 1$. So far the equation is quite generally valid. Now let us assume that we are close to the left edge, by writing $\phi' = ay - 1$. In this case the integration range for ϕ is restricted by the demand $|\tilde{\phi}| \leq 1$ to a small symmetric interval around 0. We may thus write $\rho_a(\phi) \approx \rho_a(0)$ to obtain the leading order approximation of the 1-point density $\rho_a(ay - 1)$ close to $\phi = -1$,

$$\begin{aligned} \rho_a^{(0)}(ay - 1) &= \frac{\rho_a(0)}{a} \int_{-1}^1 \rho_{aa}((ay - 1 - (1-a)T_2(\phi))/a) d\phi = \\ &= \frac{2\rho_a(0)}{a} \int_0^1 \rho_{aa}((ay - 1 - (1-a)T_2(\phi))/a) d\phi \end{aligned} \quad (9)$$

which we call ‘zeroth iterate’ (of our convolution scheme). Finally, we can change to an integration over $\tilde{\phi}$,

$$\begin{aligned} \tilde{\phi} = \frac{1}{a} (ay - 1 - (1-a)(2\phi^2 - 1)) &\Leftrightarrow \phi = \frac{1}{\sqrt{2(1-a)}} \sqrt{a(y - 1 - \tilde{\phi})} \\ d\phi &= \frac{-a d\tilde{\phi}}{2\sqrt{2a(1-a)}} \frac{1}{\sqrt{y - 1 - \tilde{\phi}}} \end{aligned} \quad (10)$$

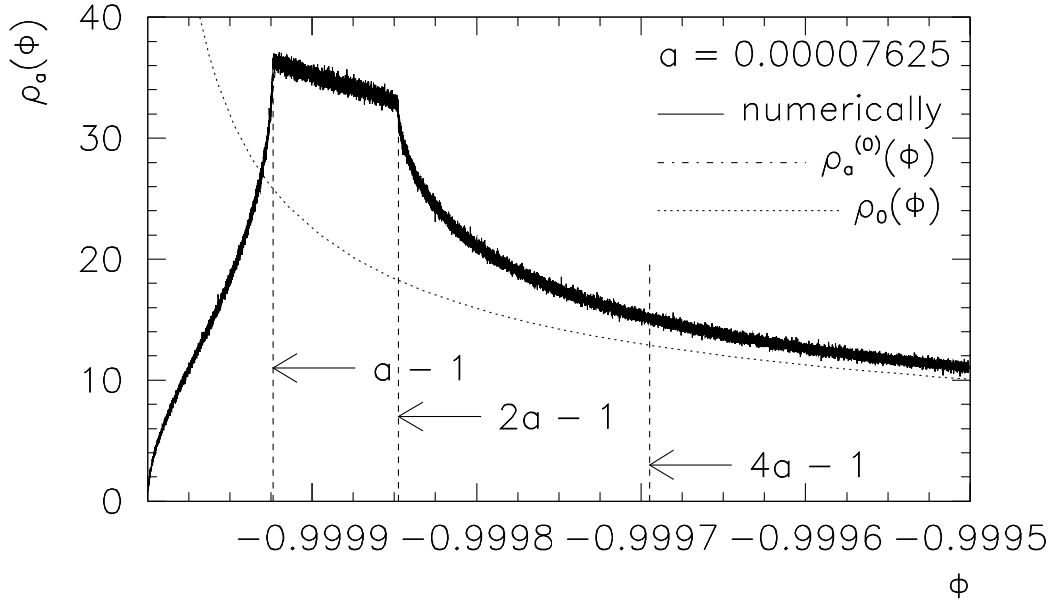


Figure 9: Invariant density $\rho_a(\phi)$ close to $\phi = -1$ for the 2B-string with $a = 0.00007625$, as compared to the invariant density $\rho_0(\phi)$ for vanishing coupling (dashed curve)

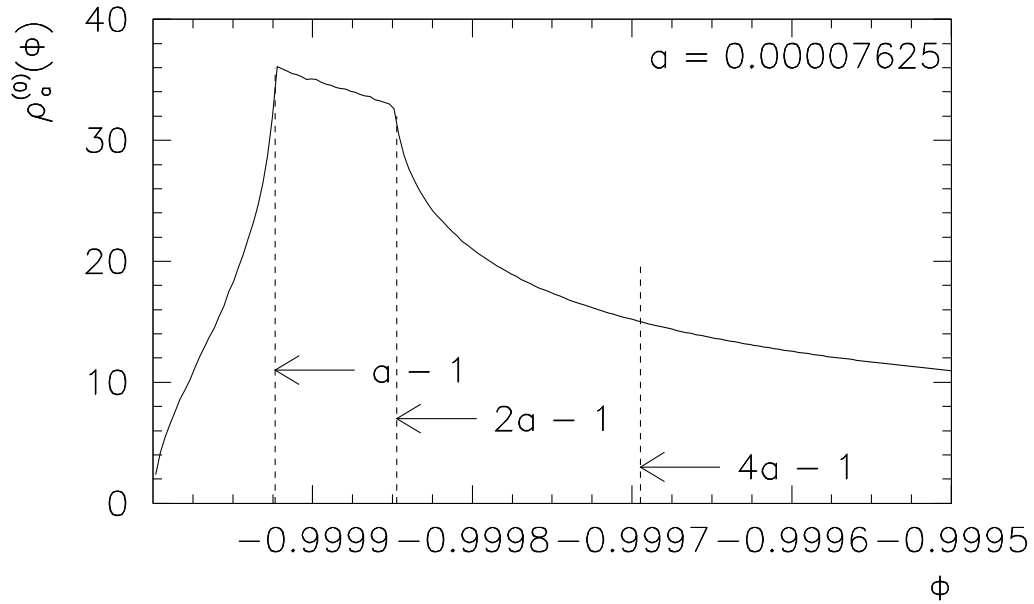


Figure 10: Zeroth iterate $\rho_a^{(0)}(\phi)$ close to $\phi = -1$, calculated according to Eq. (13)

to obtain

$$\rho_a^{(0)}(ay - 1) = \frac{\rho_a(0)}{\sqrt{2a(1-a)}} \int_{-1}^{y-1} \frac{\rho_{aa}(\tilde{\phi}) d\tilde{\phi}}{\sqrt{y-1-\tilde{\phi}}}. \quad (11)$$

Note that the integration range in this formula is given by the domain of the square root appearing in the denominator and the demand $|\tilde{\phi}| \leq 1$. In the following, we no longer write down the integration limits explicitly. Using Eq. (7) for the density of $\tilde{\phi}$, we can substitute $\phi_+ = 2\tilde{\phi} - \phi_-$ to end up with the symmetric result

$$\rho_a^{(0)}(ay - 1) = \frac{\rho_a(0)}{\sqrt{2a(1-a)}} \int \frac{\rho_a(\phi_+) d\phi_+ \rho_a(\phi_-) d\phi_-}{\sqrt{y-1 + (\phi_+ + \phi_-)/2}}. \quad (12)$$

The two integration limits in this formula are given by the condition that the argument of the square root should always be positive and that $\phi_+, \phi_- \in [-1, 1]$. Note that in calculating the leading order approximation of the density close to $\phi = -1$ there is no need to keep the indices a on the right hand side of Eq. (12). Therefore, we can use the explicit representations in Eqs. (3) and (7) to calculate the integrals. Another possibility is to calculate the integrals as time averages. We may just iterate with uncoupled Tchebyscheff maps T_2 to obtain a weighting with ρ_0 . From this we obtain

$$\rho_a^{(0)}(ay - 1) = \frac{1}{\pi \sqrt{2a(1-a)} J^2} \sum_{n_+, n_-} \frac{\theta(y-1 + (\phi_{n_+} + \phi_{n_-})/2)}{\sqrt{y-1 + (\phi_{n_+} + \phi_{n_-})/2}} \quad (13)$$

where J is the total number of iterations. The analytic perturbative result calculated in this way is shown in Fig. 10. It coincides quite perfectly with the numerically obtained density (obtained by direct iteration of the CML) as shown in Fig. 9.

The main conclusions that we can draw up to now are:

- The behaviour at the boundary close to $\phi = -1$ is reproduced by the zeroth iterate of our convolution scheme with high accuracy. To leading order in a we have $\rho_a(ay - 1) = \rho_a^{(0)}(ay - 1)$.
- For arbitrarily small a the density $\rho_a(\phi)$ does not approach infinity for $\phi \rightarrow -1$ (as in the uncoupled case) but falls off to 0 after a maximum at $\phi = a - 1$.
- If we parametrize the region close to $\phi = -1$ by $\phi = ay - 1$, the only dependence on the coupling a that is left for the density is $\rho_a(ay - 1) \sim a^{-1/2}$.

Actually, the last property is already a property of $\rho_0(\phi)$,

$$\rho_0(ay - 1) = \frac{1}{\pi \sqrt{1 - (ay - 1)^2}} \approx \frac{1}{\pi \sqrt{2ay}}. \quad (14)$$

However, in combination with the appearance of a last maximum at $\phi = a - 1$, we obtain a scaling relation between a and ϕ , which induces a variety of interesting results (see section 6).

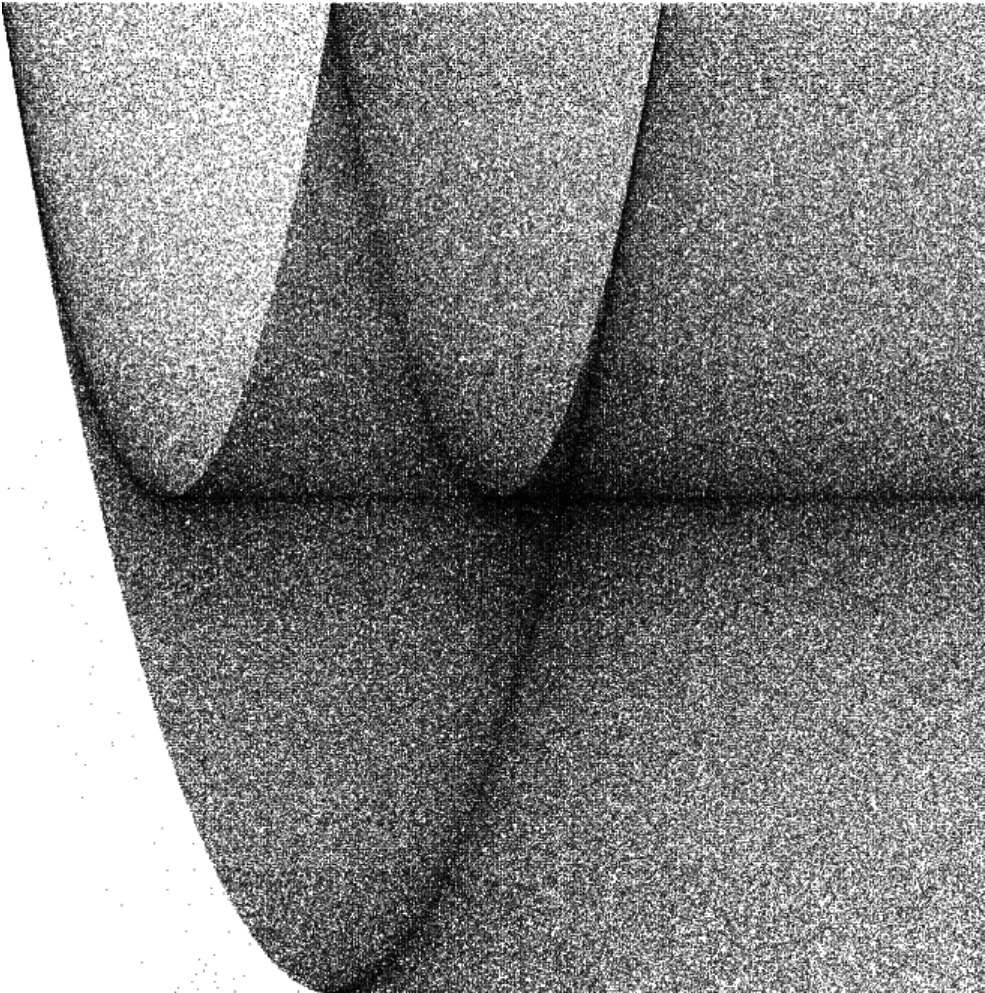


Figure 11: Two-point density function $\rho_{aa}(ay - 1, \tilde{\phi})$ in the range $0 \leq y \leq 3$ (horizontally) and $-1 \leq \tilde{\phi} \leq +1$ (vertically)

3.2 Two-point function and backstep transformation

The next iteration step of our scheme leads from the region just considered to the main scaling region close to $\phi = +1$ which we parametrize by $\phi = 1 - ax$. In order to accomplish this step we could think of again calculating the convolution according to Eq. (8), only that in this case we use $\phi' = 1 - ax$. However, for values ϕ close to the boundaries neighbored field variables exhibit strong correlations, they cannot be regarded as nearly independent anymore. The 2-point density function describing the joint probability of neighbored lattice sites exhibits a rich structure, as shown in Fig. 11. This structure at the border of the interval represents the main difficulty to analyse the invariant densities of nonhyperbolic CMLs. Our basic idea in the following is to proceed by one backward iteration to the region close to $\phi = 0$ where approximate independence holds, and then transform the densities accordingly.

In order to construct the two-point function analytically, we make use of the fact that the integral of this function $\rho_{aa}(ay - 1, \tilde{\phi})$ over $\tilde{\phi}$ has to reproduce $\rho_a(ay - 1)$ since this is just the

marginal distribution. In searching for a transformation which keeps the integral in Eq. (12) invariant but changes the integrand we have to think about an appropriate substitution. The one which fits in for our purposes is the transformation $\phi_{\pm} = T_2^{-1}(\phi'_{\pm})$ which we may call the backstep (or pre-image) transformation. The backstep transformation keeps the unperturbed density invariant,

$$\rho_0(\phi'_{\pm})d\phi'_{\pm} = \rho_0(T_N(\phi_{\pm}))dT_N(\phi_{\pm}) = N\rho_0(\phi_{\pm})d\phi_{\pm}. \quad (15)$$

Under this transformation we obtain quite generally

$$\rho_a(ay - 1) = \frac{1}{\pi\sqrt{2a(1-a)}N^2} \sum \sum \int \frac{\rho_0(\phi'_+)d\phi'_+\rho_0(\phi'_-)d\phi'_-}{\sqrt{y-1+(T_N^{-1}(\phi'_+)+T_N^{-1}(\phi'_-))/2}} \quad (16)$$

where the two-fold sum runs over all N solutions of the inverse map $T_N^{-1}(\phi)$. For $N = 2$, we sum over the two branches of each of the two square roots. In substituting finally $\phi'_+ = 2\tilde{\phi} - \phi'_-$ we obtain $\rho_a^{(0)}(ay - 1) = \int \rho_{aa}^{(0)}(ay - 1, \tilde{\phi})d\tilde{\phi}$ where

$$\rho_{aa}^{(0)}(ay - 1, \tilde{\phi}) = \frac{1}{\pi\sqrt{2a(1-a)}2^2} \sum_{\pm} \sum_{\pm} \frac{2\rho_0(2\tilde{\phi} - \phi'_-)\rho_0(\phi'_-)}{\sqrt{y-1+(\pm\sqrt{\tilde{\phi}+(1-\phi'_-)/2} \pm \sqrt{(1+\phi'_-)/2})/2}}. \quad (17)$$

This perturbative result reproduces the numerical 2-point distribution observed in Fig. 11. Finally, as a one-point distribution the function $\rho_{aa}^{(0)}(ay - 1, \tilde{\phi})$ has to be normalised. Actually, we obtain this normalisation by no effort because obviously the ratio $\hat{\rho}_{aa}^{(0)}(ay - 1, \tilde{\phi}) = \rho_{aa}^{(0)}(ay - 1, \tilde{\phi})/\rho_a^{(0)}(ay - 1)$ (describing a conditional probability) is normalised.

3.3 The first iteration step: from $\phi = -1$ to $\phi = +1$

The normalisation is skipped again if we use the conditional probability $\hat{\rho}_{aa}^{(0)}(ay - 1, \tilde{\phi})$ close to $\phi = -1$ for the calculation of the next iterate,

$$\begin{aligned} \rho_a^{(1)}(\phi') &= \int \hat{\rho}_{aa}^{(0)}(ay - 1, (\phi' - (1-a)T_2(ay - 1))/a) \rho_a^{(0)}(ay - 1)dy = \\ &= \int \rho_{aa}^{(0)}(ay - 1, (\phi' - (1-a)T_2(ay - 1))/a) dy. \end{aligned} \quad (18)$$

For $\phi' = 1 - ax$ the second argument reads $\tilde{\phi} = 1 - 4y - x + O(a)$. Because of this, the range of integration for y does not exceed $(1-x)/4$ by more than one fourth. Instead of integrating over y , we can integrate over $\tilde{\phi}$ which enables us to reverse the backstep transformation,

$$\begin{aligned} \rho_a^{(1)}(1 - ax) &= \frac{1}{4} \int \rho_{aa} \left(\frac{a}{4}(x - 1 + \tilde{\phi}) - 1, \tilde{\phi} \right) d\tilde{\phi} = \\ &= \frac{1}{4\pi\sqrt{2a(1-a)}2^2} \sum^2 \sum^2 \int \frac{2\rho_0(2\tilde{\phi} - \phi'_-)\rho_0(\phi'_-)d\tilde{\phi}d\phi'_-}{\sqrt{(x-1+\tilde{\phi})/4-1+(T_2^{-1}(2\tilde{\phi}-\phi'_-)+T_2^{-1}(\phi'_-))/2}} = \\ &= \frac{1}{4\pi\sqrt{2a(1-a)}2^2} \sum^2 \sum^2 \int \frac{\rho_0(\phi'_+)d\phi'_+\rho_0(\phi'_-)d\phi'_-}{\sqrt{(x-1+(\phi'_++\phi'_-)/2)/4-1+(T_2^{-1}(2\tilde{\phi}-\phi'_-)+T_2^{-1}(\phi'_-))/2}} \\ &= \frac{1}{4\pi\sqrt{2a(1-a)}} \sum^2 \sum^2 \int \frac{\rho_0(\phi_+)d\phi_+\rho_0(\phi_-)d\phi_-}{\sqrt{(x-1+(T_2(\phi_+)+T_2(\phi_-))/2)/4-1+(\phi_++\phi_-)/2}} = \end{aligned}$$

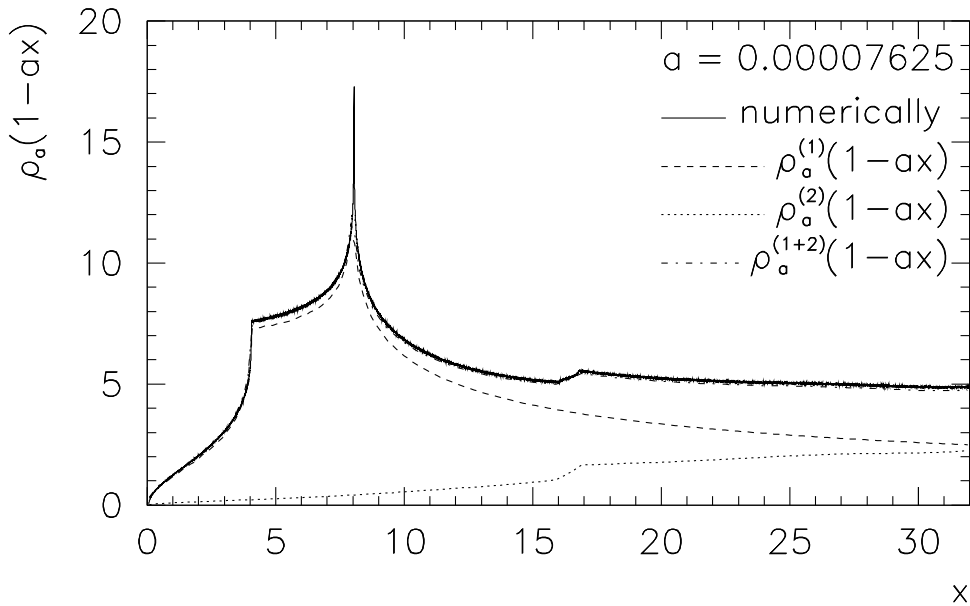


Figure 12: 1-point density $\rho_a(1 - ax)$ at the right edge of the interval (solid curve) for the 2B-string with $a = 0.00007625$ as a function of x , compared to the first iterate $\rho_a^{(1)}(1 - ax)$ (dashed curve), the second iterate $\rho_a^{(2)}(1 - ax)$ (dotted curve), and the sum of both (dashed-dotted curve)

$$= \frac{1}{4\pi\sqrt{2a(1-a)}} \int \frac{\rho_0(\phi_+)d\phi_+\rho_0(\phi_-)d\phi_-}{\sqrt{x/4 + (\phi_+ + \phi_- - 2)/2 + (T_2(\phi_+) + T_2(\phi_-) - 2)/8}}. \quad (19)$$

The sums over the branches disappears again. For the last line we have used an equivalent representation which will later allow us to unify the results. Again, we can use a time average over iterates of uncoupled Tchebyscheff maps to generate the weighting with the density ρ_0 in the above integrals.

3.4 Further iteration steps

As one can see in Fig. 12, the first iterate of our convolution scheme as given by Eq. (19) already fits the invariant density reasonably well. However, it does not reproduce the structure near $x = 16 \dots 17$. Since T_2 has an unstable fixed point at $\phi = 1$ with slope $+4$, this structure is a consequence of local iterates of the CML passing the previously described correlated border area one step earlier.

In a recursive way, we thus define density contributions (iterates of our convolution scheme) $\rho_a^{(p)}(1 - ax)$ ($p > 1$) as follows:

- perform the backstep transformation
- calculate the two-point function $\rho_{aa}^{(p-1)}(1 - ax', \tilde{\phi})$ by integrating over ϕ'_-
- normalise by $\rho_a^{(p-1)}(1 - ax')$

- integrate over x' (the normalisation cancels)
- retract the backstep transformation

Following this recipe, we obtain

$$\rho_a^{(p)}(1 - ax) = \frac{1}{4^p \pi \sqrt{2a(1-a)}} \int \frac{\rho_0(\phi_+) d\phi_+ \rho_0(\phi_-) d\phi_-}{\sqrt{x/4^p + r_2^p(\phi_+) + r_2^p(\phi_-)}}, \quad r_2^p(\phi) := \frac{1}{2} \sum_{q=0}^p \frac{T_{2^q}(\phi) - 1}{4^q}. \quad (20)$$

The entire invariant density is given by the sum over all these contributions,

$$\rho_a(1 - ax) = \sum_{p=1}^{\infty} \rho_a^{(p)}(1 - ax) = \sum_{p=1}^{\infty} \frac{1}{4^p \pi \sqrt{2a(1-a)}} \int \frac{\rho_0(\phi_+) d\phi_+ \rho_0(\phi_-) d\phi_-}{\sqrt{x/4^p + r_2^p(\phi_+) + r_2^p(\phi_-)}}. \quad (21)$$

The series converges rapidly, so usually it is sufficient to take into account the first few functions $\rho_a^{(p)}$ only. Roughly speaking, the contribution $\rho_a^{(p)}$ takes care of those points that passed the nonhyperbolic region p steps ago.

Apparently Eq. (20) does even hold for the case $p = 0$, taking into account that the integral is invariant under the replacements $\phi_{\pm} \rightarrow -\phi_{\pm}$. However, in this case the left hand side has to be $\rho_a^{(0)}(ax - 1)$, i.e. the zeroth iterative of our scheme located close to $\phi = -1$.

Fig. 12 shows our analytic results $\rho_a^{(1)}(1 - ax)$, $\rho_a^{(2)}(1 - ax)$ and the sum of these two contributions. There is excellent agreement with the numerical histogram. The agreement is so good that the sum of the two terms is not visible behind the numerical data points.

4 Explaining the selfsimilar shape of the density patterns

It is obvious that the square root in the denominator of Eq. (21) has essential influence on the shape of the invariant 1-point density of the CML, since the argument of the square root needs to be positive which determines the integration range in our formulas. Abrupt changes of the density pattern are connected to zero-border crossings of the arguments of the square roots. Looking more closely at the function

$$r_2^p(\phi_+, \phi_-, x) = \frac{x}{4^p} + r_2^p(\phi_+) + r_2^p(\phi_-), \quad (22)$$

we can find reasons for the patterns. In order to do this analysis, we generated the contour plots of $r_2^p(\phi_+) + r_2^p(\phi_-)$ for the values $p = 0, 1, 2, 3$ by using MATHEMATICA. These plots are shown in Fig. 13. It is obvious that the demand $r_2^p(\phi_+, \phi_-, x) \geq 0$ describes a nontrivial limitation of the basic integration range $\phi_{\pm} \in [-1, 1]$. The equation $r_2^p(\phi_+, \phi_-, x) = 0$ for different values of x describes the analytic curves which appear as contour curves in Fig. 13.

4.1 Patterns generated by $p = 0$

The analytic curve given by the vanishing of the radical

$$r_2^0(\phi_+, \phi_-, y) = y + r_2^0(\phi_+) + r_2^0(\phi_-) = y + (\phi_+ + \phi_-)/2 - 1 \quad (23)$$

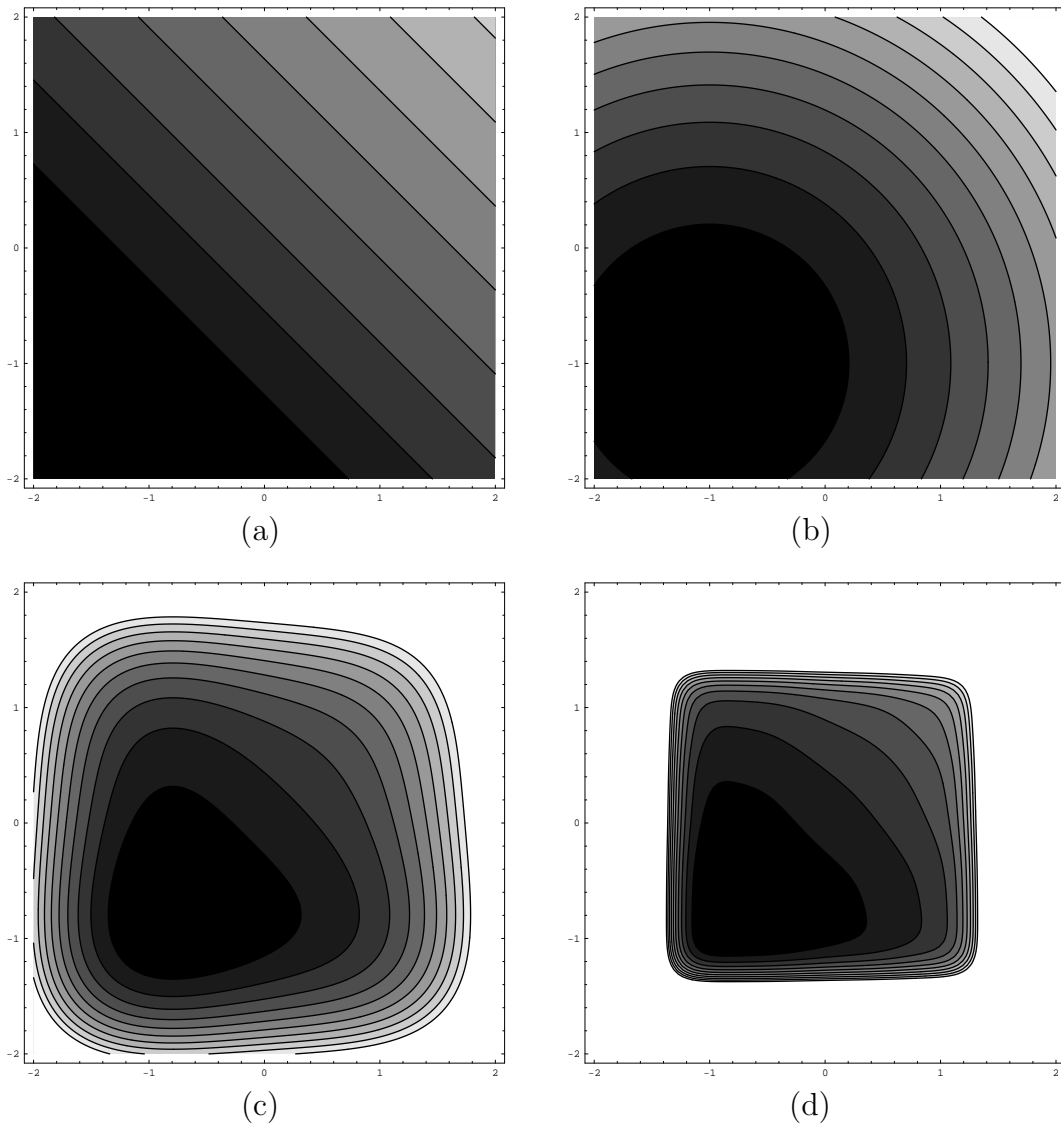


Figure 13: Contour plots of the function $r_2^p(\phi_+) + r_2^p(\phi_-)$ for the values $p = 0$ (a), $p = 1$ (b), $p = 2$ (c), and $p = 3$ (d) in the range given by $\phi_{\pm} \in [-2, 2]$. Dark shadings indicate low values, bright shadings high values of the function in $[-2, 2]$

describes an off-diagonal straight line with intercept $2(y - 1)$ that limits the integration range to lower values of ϕ_+ and ϕ_- (cf. Fig. 13(a)). We observe that for $y = 0$ the basic integration range is totally suppressed, the integration area then increases like $(2y)^2/2$ up to $y = 1$ and like $(4+(2-y)^2)/2$ up to $y = 2$. Starting from $y = 2$, the basic integration range is no longer limited by the constraint $r_2^0(\phi_+, \phi_-, y) \geq 0$. In accordance to this, the zeroth-order density contribution starts with the value zero at $y = 0$, shows non-differentiable cusps at $y = 1$ and $y = 2$ and monotonic behaviour elsewhere (compare Fig. 9).

4.2 Patterns generated by $p = 1$

Here we need to analyse the radical

$$r_2^1(\phi_+, \phi_-, x) = \frac{x}{4} + r_2^1(\phi_+) + r_2^1(\phi_-) = \frac{1}{4} \left(x + (\phi_+ + 1)^2 + (\phi_- + 1)^2 - 8 \right), \quad (24)$$

For $x < 8$ the analytic curve parametrized by $r_2^1(\phi_+, \phi_-, x) = 0$ is a circle in the (ϕ_+, ϕ_-) -plane with radius $\sqrt{8-x}$ and center located at $(-1, -1)$ (cf. Fig. 13(b)). The intersection of the outside of this circle and the inside of the rectangle $-1 \leq \phi_{\pm} \leq 1$ determines the integration range.

- For $x = 0$ the rectangle is totally covered by the circle. In this case, the integration range vanishes. We see that the $p = 1$ density contribution vanishes for $x = 0$ as well.
- Between $x = 0$ and $x = 4$ the circle uncovers the two positive edges of the rectangle, given by the lines $\phi_{\pm} = +1$. We see that the $p = 1$ density contribution grows monotonically in this interval.
- Between $x = 4$ and $x = 8$ the circle uncovers also the two negative edges of the rectangle, given by the lines $\phi_{\pm} = -1$. In this interval the $p = 1$ density contribution declines.
- Above $x = 8$ the whole rectangle is uncovered, so there is no restriction of the integration range anymore. Starting from $x = 8$ there are no further cusps. Caused by the increasing denominator, the $p = 1$ density contribution declines.

4.3 Patterns generated by $p = 2$

The second iterate $\rho_a^{(2)}(1 - ax)$ shown in Fig. 12 has a cusp at $x = 17$ which is responsible for the shift of the cusp of the invariant density by an amount of $-\log_4(17/16)$ in Fig. 6. In a similar way as for $p = 1$, we can proceed for $p = 2$. The only point is that we do no longer have a name for the algebraic curve described by $r_2^2(\phi_+, \phi_-, x) = 0$. However, the behaviour is similar as the shape of the curve is a kind of mixture between a circle, a rectangle and a triangle (cf. Fig. 13(c)). If we analyse the analytic curve for $p = 2$ more closely, we find that the positive edges of the rectangle constituting the basic integration range are fully uncovered not at $x = 16$ as could be assumed for the circle but at $x = 17$. However, starting from $x = 16$ the positive edges start to be uncovered from the negative side. Therefore, we obtain the two cusps at $x = 16$ and $x = 17$ as observed. Finally, the basic integration range becomes totally uncovered for a value $x \approx 33.524$, giving rise to a last cusp of this pattern at distance $-\log_4(x/16) \approx -0.534$ from the first cusp (corresponding to $x = 16$).

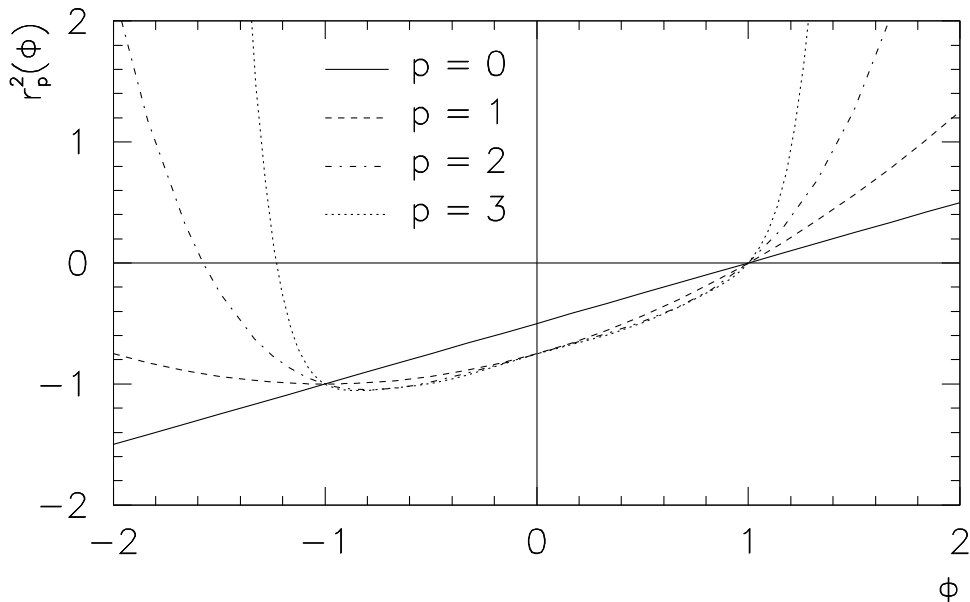


Figure 14: the function $r_2^p(\phi)$ for the values $p = 0, 1, 2, 3$

4.4 Patterns generated by $p \geq 3$

If we look at the function $r_2^p(\phi)$ for even higher values of p we make an interesting observation. While for the outside region $|\phi| > 1$ the function $r_2^p(\phi)$ starts to diverge, it rapidly converges to a limiting function inside the region $|\phi| \leq 1$. This behaviour is shown in Fig. 14. Only the inside region is essential for the integration. Therefore, we can conclude that $r_2^p(\phi) \approx r_2^\infty(\phi)$ for relatively small p and $|\phi| \leq 1$. As a consequence of this, there is invariance of the patterns generated by the higher iterates of our scheme under the replacement $x \rightarrow x/4$. As a general observation for the radical function $r_2^p(\phi)$ we add that $r_2^p(\phi + 1) = 0$, $r_2^p(\phi = 0) = -1/2$, and $r_2^p(-\phi) = r_2^p(\phi) - \phi$ which is caused by the symmetry property of the Tchebyscheff polynomial $T_2(\phi)$ and its iterates $T_{2^q}(\phi) = T_2(T_{2^{q-1}}(\phi))$.

5 The scaling behaviour for coupled 3rd order Tchebyscheff maps

All the steps we have performed in order to explain the scaling behaviour of the 2B-string can be performed for the 3B-string (coupled 3rd-order Tchebyscheff maps with $s = 1, b = 0$) as well. Scaling regions of the density are transferred by convolution,

$$\rho_a(\phi') = \frac{1}{a} \int \rho_a(\phi) \rho_{aa}((\phi' - (1-a)T_3(\phi))/a) d\phi. \quad (25)$$

However, in order to integrate over the argument $\tilde{\phi}$ of the density $\rho_{aa}(\tilde{\phi})$ we have to solve the cubic equation

$$T_3(\phi) = 4\phi^3 - 3\phi = \frac{\phi' - a\tilde{\phi}}{1-a} =: \hat{\phi}. \quad (26)$$

The three real solutions are

$$\begin{aligned}
\phi_+ &= \cos\left(\frac{1}{3}\arccos\hat{\phi}\right), & +\frac{1}{2} \leq \phi_0 \leq +1 \\
\phi_0 &= \cos\left(\frac{1}{3}\arccos\hat{\phi} + \frac{2\pi}{3}\right), & -\frac{1}{2} \leq \phi \leq +\frac{1}{2} \\
\phi_- &= \cos\left(\frac{1}{3}\arccos\hat{\phi} + \frac{4\pi}{3}\right), & -1 \leq \phi \leq -\frac{1}{2}
\end{aligned} \tag{27}$$

describing the three branches of the inverse map $T_3^{-1}(\hat{\phi})$ (similar formulas apply, of course, to the N -th order Tchebyscheff map, where there are N real solutions). In order to replace the differential $d\phi$ in Eq. (25) by $d\tilde{\phi}$, we have to specify which of the branches are involved. The demand $|\tilde{\phi}| \leq 1$ leads to

$$\frac{\phi' - a}{1 - a} \leq \hat{\phi} \leq \frac{\phi' + a}{1 - a}. \tag{28}$$

5.1 Iterates close to $\phi = +1$

If we use $\phi' = 1 - ax$, $\hat{\phi}$ is restricted by

$$1 - ax \approx \frac{1 - a(1 + x)}{1 - a} \leq \hat{\phi} \leq \frac{1 + a(1 - x)}{1 - a} \approx 1 + a(2 - x) \tag{29}$$

and by $-1 \leq \hat{\phi} \leq +1$. $\hat{\phi}$ turns out to be almost $+1$, its pre-images under the Tchebyscheff map $\hat{\phi} = T_3(\phi)$ are found at $\phi = +1$ and $\phi = -1/2$. The unperturbed starting contribution of our convolution scheme, therefore, comes from $\phi = -1/2$, involving the branches ϕ_0 and ϕ_- . We obtain (for $\hat{\phi} \approx 1$)

$$d\phi_0 = -\sin\left(\frac{1}{3}\arccos\hat{\phi} + \frac{2\pi}{3}\right) \frac{-d\hat{\phi}}{3\sqrt{1 - \hat{\phi}^2}} \approx \frac{d\hat{\phi}}{2\sqrt{3(1 - \hat{\phi}^2)}}, \tag{30}$$

$$d\phi_- = -\sin\left(\frac{1}{3}\arccos\hat{\phi} + \frac{4\pi}{3}\right) \frac{-d\hat{\phi}}{3\sqrt{1 - \hat{\phi}^2}} \approx \frac{-d\hat{\phi}}{2\sqrt{3(1 - \hat{\phi}^2)}}. \tag{31}$$

Starting with the integration range for $\hat{\phi}$ as indicated before, both integrations over ϕ_0 and ϕ_- are mapped onto this integration range. If we take into account that the integration range for ϕ_0 declines from $\phi = -1/2$ to lower values, we can combine both $d\phi_0$ and $d\phi_-$ to obtain

$$d\phi = \frac{-d\hat{\phi}}{\sqrt{3(1 - \hat{\phi}^2)}} = \frac{a d\tilde{\phi}}{(1 - a)\sqrt{3(1 - (1 - ax - a\tilde{\phi})^2/(1 - a)^2)}} \approx \frac{a d\tilde{\phi}}{\sqrt{6a(x - 1 + \tilde{\phi})}} \tag{32}$$

where we inserted $\hat{\phi}$ for $\phi' = 1 - ax$ and calculated the leading order approximation in a . Again, the right hand side of Eq. (25) needs to be calculated only to leading order in a . Therefore, we replace all density indices on this side by 0. Finally, as ϕ is close to $\phi = -1/2$, we can replace $\rho_0(\phi)$ by the constant value $\rho_0(-1/2) = 2/\pi\sqrt{3}$ to obtain the zeroth iterate

$$\begin{aligned}
\rho_a^{(0)}(1 - ax) &= \frac{2}{3\pi\sqrt{2a}} \int \frac{\rho_{00}(\tilde{\phi})d\tilde{\phi}}{\sqrt{x - 1 + \tilde{\phi}}} = \frac{2}{3\pi\sqrt{2a}} \int \frac{2\rho_0(2\tilde{\phi} - \phi_-)\rho_0(\phi_-)d\tilde{\phi}d\phi_-}{\sqrt{x - 1 + \tilde{\phi}}} = \\
&= \frac{2}{3\pi\sqrt{2a}} \int \frac{\rho_0(\phi_+)d\phi_+\rho_0(\phi_-)d\phi_-}{\sqrt{x - 1 + (\phi_+ + \phi_-)/2}}. & (\phi_+ = 2\tilde{\phi} - \phi_-)
\end{aligned} \tag{33}$$

The zeroth-order two-point density function $\rho_{aa}^{(0)}(\phi, \tilde{\phi})$ is obtained by the backstep transformation

$$\rho_a^{(0)}(1 - ax) = \frac{2}{3\pi\sqrt{2a}} \frac{1}{3^2} \sum^3 \sum^3 \int \frac{\rho_0(\phi'_+) d\phi'_+ \rho_0(\phi'_-) d\phi'_-}{\sqrt{x - 1 + (T_3^{-1}(\phi'_+) + T_3^{-1}(\phi'_-))/2}}. \quad (34)$$

The first iterate of our convolution scheme is again the integral of the two-point function,

$$\rho_a^{(1)}(1 - ax) = \int \rho_{aa}^{(0)}(1 - ax', \tilde{\phi}') dx' \quad (35)$$

where

$$\tilde{\phi}' = \frac{1}{a} ((1 - ax) - (1 - a)T_3(1 - ax')) \approx 9x' + 1 - x. \quad (36)$$

Integrating over $\tilde{\phi}'$ instead of x' and substituting $\tilde{\phi}' = (\phi'_+ + \phi'_-)/2$, we can again revert the backstep transformation to obtain the first iterate

$$\rho_a^{(1)}(1 - ax) = \frac{2}{27\pi\sqrt{2a}} \int \frac{\rho_0(\phi_+) d\phi_+ \rho_0(\phi_-) d\phi_-}{\sqrt{x/9 + (\phi_+ + \phi_- - 2)/2 + (T_3(\phi_+) + T_3(\phi_-) - 2)/18}}. \quad (37)$$

Continuing in the same manner, we obtain

$$\rho_a(1 - ax) = \sum_{p=0}^{\infty} \rho_a^{(p)}(1 - ax) = \sum_{p=0}^{\infty} \frac{2}{9^p 3\pi\sqrt{2a}} \int \frac{\rho_0(\phi_+) d\phi_+ \rho_0(\phi_-) d\phi_-}{\sqrt{x/9^p + r_3^p(\phi_+) + r_3^p(\phi_-)}} \quad (38)$$

where

$$r_3^p(\phi) = \frac{1}{2} \sum_{q=0}^p \frac{T_{3^q}(\phi) - 1}{9^q}. \quad (39)$$

5.2 Iterates close to $\phi = -1$

We no longer have to go into details for the calculation close to the lower boundary $\phi = -1$. The unperturbed domain for the zeroth iterate is given by a region close to $\phi = +1/2$, the higher iterates remain close to $\phi = -1$. The final result reads

$$\rho_a(ay - 1) = \sum_{p=0}^{\infty} \rho_a^{(p)}(ay - 1) = \sum_{p=0}^{\infty} \frac{2}{9^p 3\pi\sqrt{2a}} \int \frac{\rho_0(\phi_+) d\phi_+ \rho_0(\phi_-) d\phi_-}{\sqrt{y/9^p + r_3^p(\phi_+) + r_3^p(\phi_-)}}. \quad (40)$$

We obtain $\rho_a(ay - 1) = \rho_a(1 - ay)$, i.e. there is symmetry of the 1-point density as expected from general principles [4]. Finally, we add the remark that the zeroth iterate for the 3B-string close to the lower boundary $\phi = -1$ should coincide (up to a general factor) with the zeroth iterate (and, therefore, with the density) of the 2B-string close to $\phi = -1$, see section 5.4 for a numerical check of this fact.

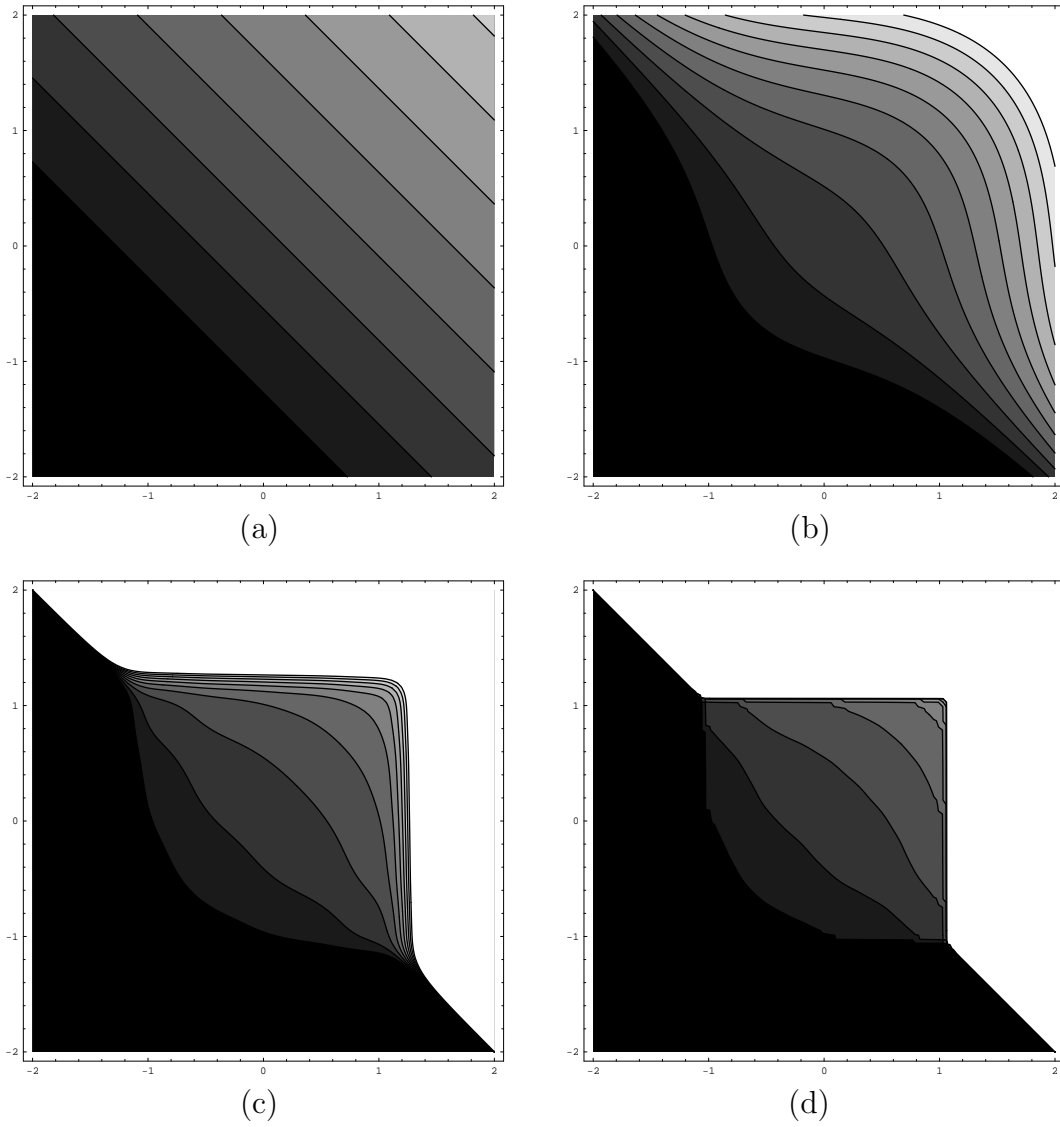


Figure 15: Contour plots of the function $r_3^p(\phi_+) + r_3^p(\phi_-)$ for the values $p = 0$ (a), $p = 1$ (b), $p = 2$ (c), and $p = 3$ (d) in the range given by $\phi_{\pm} \in [-2, 2]$. Dark shadings indicate low values, bright shadings high values of the function in $[-2, 2]$

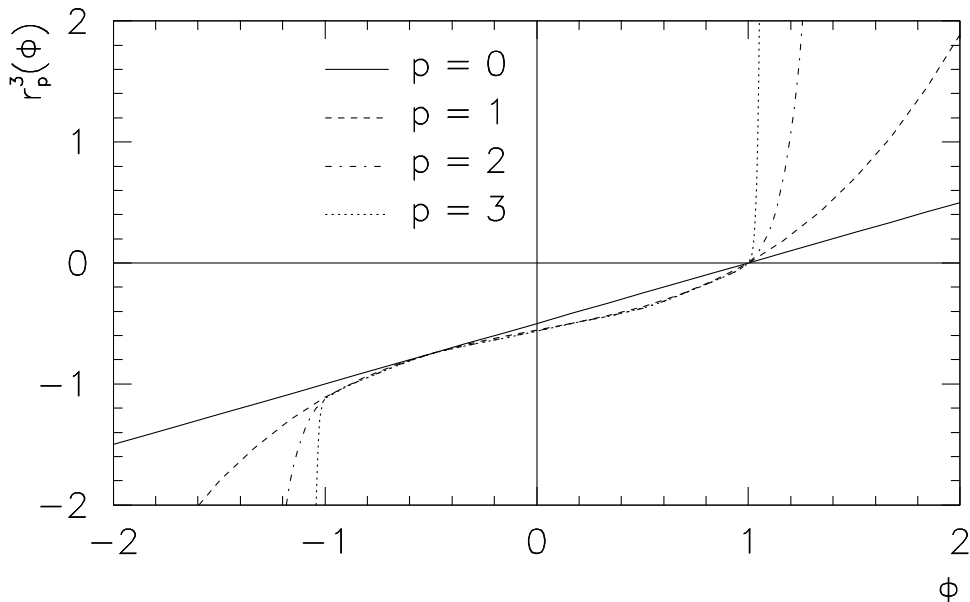


Figure 16: the function $r_3^p(\phi)$ for the values $p = 0, 1, 2, 3$

5.3 The 3B-pattern

What to predict about the 3B-pattern? In Fig. 15 we display the contour plots of the function $r_3^p(\phi_+) + r_3^p(\phi_-)$ for the values $p = 0, 1, 2, 3$. There is a step in passing the off-diagonal for $|\phi_{\pm}| > 1$, whose size increases with p . However, in the region relevant for the integration ($-1 \leq \phi_{\pm} \leq +1$) the function converges. In Fig. 16 we show $r_3^p(\phi)$ for the same values $p = 0, 1, 2, 3$. Up to a shift which is given by

$$r_3^p(0) = -\frac{1}{2} \sum_{q=0}^p \frac{1}{9^q} = -\frac{1 - (1/9)^{p+1}}{2(1 - 1/9)} \xrightarrow{p \rightarrow \infty} -\frac{9}{16}, \quad (41)$$

the odd symmetry of the Tchebyscheff polynomial $T_3(\phi)$ and its iterates $T_{3^q}(\phi) = T_3(T_{3^{q-1}}(\phi))$ cause $r_3^p(\phi) - r_3^p(0)$ to have odd symmetry. On the other hand, as in case of the 2B-string we have $r_3^p(\phi = +1) = 0$ because of $T_{3^q}(\phi = +1) = +1$. Taking these two facts into account, we can determine the values of $r_3^p(\phi)$ at $\phi = -1$ to be two times the value at $\phi = 0$. Analysing finally the inequality $x/9^p + r_3^p(\phi_+) + r_3^p(\phi_-) > 0$ that determines the restriction of the basic integration range $-1 \leq \phi_{\pm} \leq +1$, we can understand the position of the cusps of the density curve.

- For $p = 0$ the restriction reads $x - 1 + (\phi_+ + \phi_-)/2 > 0$. The pattern turns out to be the same as for the 2B-string. We obtain full cover for $x = 0$ (i.e. full suppression of the integration range), half cover for $x = 1$, and the disappearance of the covering triangle from the basic (rectangular) integration range for $x = 2$. This reproduces the three observed segments of the density curve.
- For $p = 1$ the restriction reads $x - 10 + 2\phi_+^3 + 3\phi_+ + 2\phi_-^3 + 3\phi_- > 0$. Therefore, we should obtain half cover at $x = 10$ and disappearance of the cover for $x = 20$.

- For high (p -th) iterates, we can apply the limit in Eq. (41). We observe that the half cover should be reached for $x = (9/8)9^p$, the disappearance of the cover for $x = (9/4)9^p$. All these numbers determine non-differentiable points of the density.

5.4 Comparison with numerical results

As we did in Sec. 2, for numerical purposes it is useful to analyse the adjusted energy difference $a^{-1/2}\rho_0(\phi)\Delta\epsilon(\phi)$ as a convenient observable for which we can visualise the scaling behaviour in $\phi^* = -\log_9(1-\phi)$ close to $\phi = +1$ (because of the symmetry of the spectral density $\rho_a(\phi)$ in case of the 3B-string, the observation of the region close to $\phi = -1$ gives the same result and, therefore, is obsolete). In Fig. 17 (corresponding to Fig. 4 of the 2B-string) we show logarithmic plots of $a^{-1/2}\rho_0(\phi)\Delta\epsilon(\phi)$ for the three values $a = 0.0000476025$, $a = 0.00000528917$, and $a = 0.000000587685$ of the coupling. The various iterates of our convolution scheme are shown in Fig. 18, which corresponds to Fig. 6. We observe

- for $p = 0$ two cusps at $-\log_9(ax) = -\log_9(a)$ and $-\log_9(2a)$
- for $p = 1$ the shift of these cusps by an amount of $-\log_9(10/9) = -0.048\dots$
- for $p \geq 2$ the shift by an amount of $-\log_9(9/8) = -0.054\dots$

Finally, in Fig. 19 we compare the numerical result for the invariant density $\rho_a(1-ax)$ (solid curve) with the zeroth iterate $\rho_a^{(0)}(1-ax)$ (dashed curve), the first iterate $\rho_a^{(1)}(1-ax)$ (dotted curve), and the sum of both (dashed-dotted curve). The accuracy of the agreement is again so high that one is not able to distinguish between the solid and the dashed-dotted curve.

6 Proof of the scaling behaviour in a

At the end of this paper, having all the necessary results at hand, let us finally prove that scaling in ϕ implies scaling in a . To be more definite, we prove in the following that if $V(\phi)$ is a generic test function, then the difference of expectation values taken with invariant densities for small coupling a and vanishing coupling $a = 0$ scales with \sqrt{a} and exhibits log-periodic oscillations of period $\log N^2$:

$$\langle V(\phi) \rangle_a - \langle V(\phi) \rangle_0 = \sqrt{a} f_V(\log_{N^2}(a)), \quad f_V(x^* + 1) = f_V(x^*). \quad (42)$$

Examples of this oscillating behaviour were shown in Fig. 1.

6.1 Scaling of $\rho_a(1-ax)$ in a

To summarise, we found in section 3 that in leading order in a

$$\rho_a(1-ax) = \frac{2}{N\pi\sqrt{2a}} \sum_{p=0,1}^{\infty} \int \frac{\rho_0(\phi_+)d\phi_+\rho_0(\phi_-)d\phi_-}{N^{2p}\sqrt{x/N^{2p} + r_N^p(\phi_+) + r_N^p(\phi_-)}}, \quad N = 2, 3 \quad (43)$$

The sum starts at $p = 0$ for $N = 3$ and at $p = 1$ for $N = 2$. Thus we have

$$\rho_a(1-ax) = \frac{1}{\sqrt{a}}g(x) \quad (44)$$

where the function $g(x)$ is independent of a for small a .

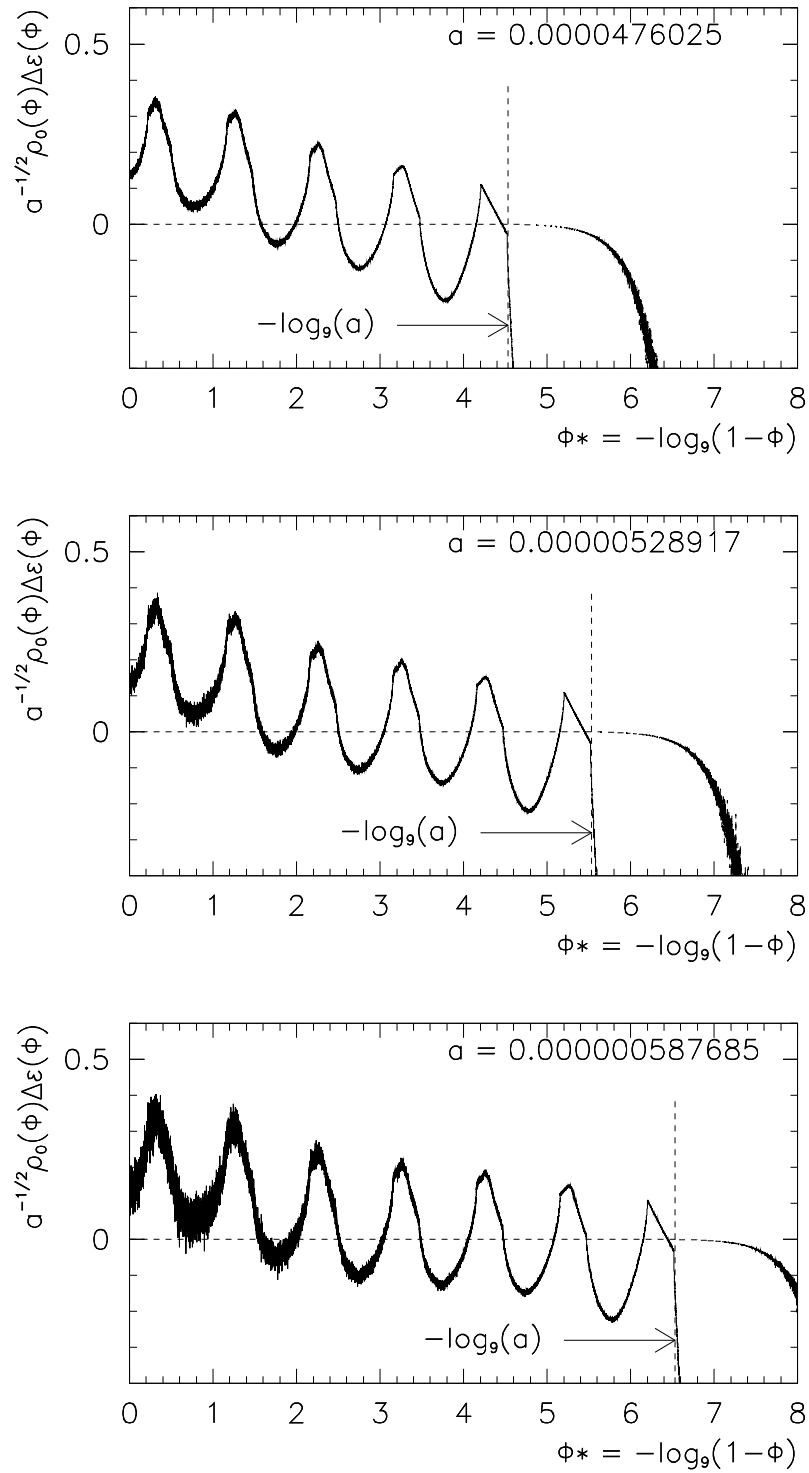


Figure 17: Adjusted energy difference $a^{-1/2} \rho_0(\phi) \Delta \epsilon(\phi)$ of the 3B-string for $a = 0.0000476025$, $a = 0.00000528917$, and $a = 0.000000587685$ (from top to bottom). Also indicated is the breakdown point of the pattern at $\phi^* = a^* = -\log_9(a)$ (vertical line).

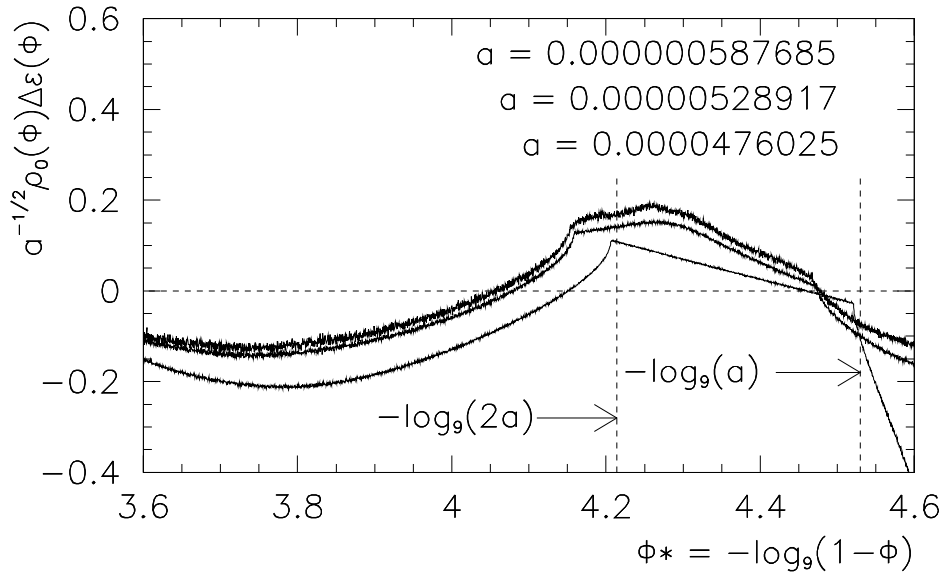


Figure 18: Adjusted energy difference $a^{-1/2}\rho_0(\phi)\Delta\epsilon(\phi)$ for the 3B-string at $a = 0.0000476025$, $a = 0.00000528917$, and $a = 0.000000587685$ (from bottom to top).

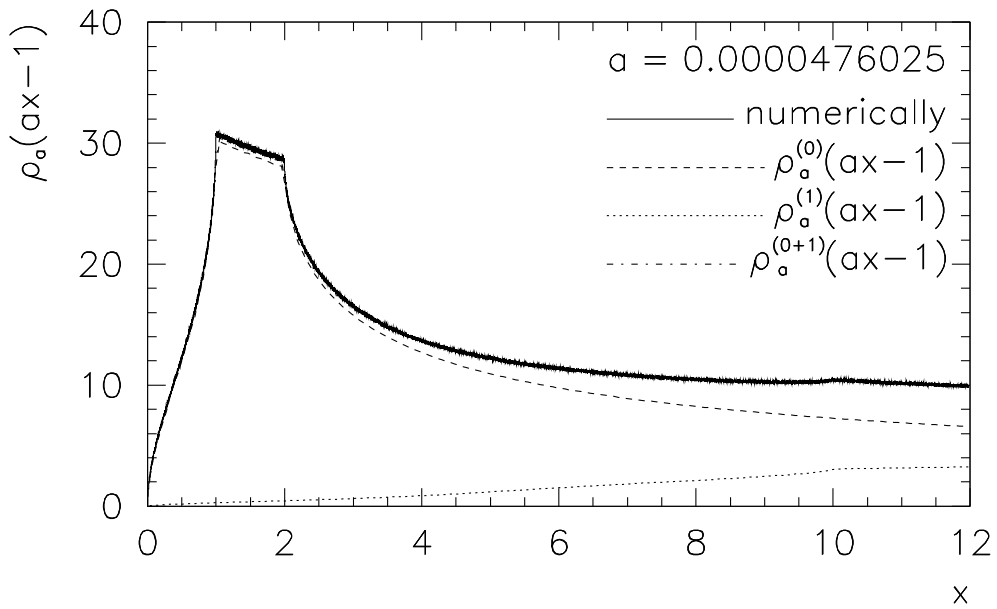


Figure 19: 1-point density $\rho_a(1 - ax)$ (solid curve) of the 3B-string for $a = 0.0000476025$ as a function of x , compared to the zeroth iterate $\rho_a^{(0)}(1 - ax)$ (dashed curve), the first iterate $\rho_a^{(1)}(1 - ax)$ (dotted curve), and the sum of both (dashed-dotted curve)

6.2 Scaling of $\rho_a(1 - ax)$ in ϕ

We observed that the adjusted energy difference $a^{-1/2}\rho_0(\phi)\Delta\epsilon(\phi)$ scales as

$$a^{-1/2}\rho_0(\phi)\Delta\epsilon(\phi) = \frac{2\pi}{N\sqrt{2}}f^*\left(-\log_{N^2}\left(\frac{1-\phi}{a}\right)\right), \quad f^*(x^* - 1) = f^*(x^*) \quad (45)$$

close to $\phi = +1$ (the constant prefactor is chosen for later convenience). If we write

$$\Delta\epsilon(\phi) = \epsilon_a(\phi) - \epsilon_0(\phi) = \frac{1}{2\pi^2\rho_0^2(\phi)} - \frac{1}{2\pi^2\rho_a^2(\phi)}, \quad (46)$$

we can expand $\rho_a(\phi) = \rho_0(\phi)(1 - 2\pi^2\rho_0^2(\phi)\Delta\epsilon(\phi))^{-1/2}$ to obtain

$$\begin{aligned} \rho_a(\phi) &\approx \rho_0(\phi)\left(1 + \pi^2\rho_0^2(\phi)\Delta\epsilon(\phi)\right) = \\ &\approx \rho_0(\phi) + \frac{2\pi^3\sqrt{a}}{N\sqrt{2}}\rho_0^2(\phi)f^*\left(-\log_{N^2}\left(\frac{1-\phi}{a}\right)\right). \end{aligned} \quad (47)$$

In order to prove the periodicity property $f^*(x^* - 1) = f^*(x^*)$ we use the fact that we can represent the invariant density $\rho_0(1 - ax)$ by a series expansion analogue to Eq. (43),

$$\begin{aligned} \rho_0(1 - ax) &= \frac{1}{\pi\sqrt{1 - (1 - ax)^2}} \frac{2}{N} \sum_{p=0,1}^{\infty} \frac{1}{N^p} \approx \frac{2}{N\pi\sqrt{2a}} \sum_{p=0,1}^{\infty} \frac{1}{N^{2p}\sqrt{x/N^{2p}}} = \\ &= \frac{2}{N\pi\sqrt{2a}} \sum_{p=0,1}^{\infty} \int \frac{\rho_0(\phi_+)d\phi_+\rho_0(\phi_-)d\phi_-}{N^{2p}\sqrt{x/N^{2p}}}. \end{aligned} \quad (48)$$

In terms of $f(x) = f^*(-\log_{N^2}(x)) = f^*(x^*)$ the periodicity reads $f(N^2x) = f(x)$. The function $f(x)$ is given by

$$f(x) = x \sum_{p=0,1}^{\infty} \int \left(\frac{\rho_0(\phi_+)d\phi_+\rho_0(\phi_-)d\phi_-}{N^{2p}\sqrt{x/N^{2p} + r_N^p(\phi_+) + r_N^p(\phi_-)}} - \frac{\rho_0(\phi_+)d\phi_+\rho_0(\phi_-)d\phi_-}{N^{2p}\sqrt{x/N^{2p}}} \right) = \sum_{p=0,1}^{\infty} f_p(x). \quad (49)$$

The periodicity can be shown for values $x \gg N^{2P}$ where P again is chosen large enough to guarantee the p -independence of the function $r_N^p(\phi)$, $r_N^p(\phi_{\pm}) \approx r_N^{\infty}(\phi_{\pm})$ for $p \geq P$. For this range of values for x we have

$$\begin{aligned} f_p(N^2x) &= N^2x \int \left(\frac{\rho_0(\phi_+)d\phi_+\rho_0(\phi_-)d\phi_-}{N^{2p}\sqrt{N^2x/N^{2p} + r_N^{\infty}(\phi_+) + r_N^{\infty}(\phi_-)}} - \frac{\rho_0(\phi_+)d\phi_+\rho_0(\phi_-)d\phi_-}{N^{2p}\sqrt{N^2x/N^{2p}}} \right) = \\ &= x \int \left(\frac{\rho_0(\phi_+)d\phi_+\rho_0(\phi_-)d\phi_-}{N^{2(p-1)}\sqrt{x/N^{2(p-1)} + r_N^{\infty}(\phi_+) + r_N^{\infty}(\phi_-)}} - \frac{\rho_0(\phi_+)d\phi_+\rho_0(\phi_-)d\phi_-}{N^{2(p-1)}\sqrt{x/N^{2(p-1)}}} \right) = f_{p-1}(x). \end{aligned} \quad (50)$$

On the other hand, for $p < P$ the value of x/N^{2p} is large. Therefore, we can expand the radicals,

$$\begin{aligned} \frac{1}{\sqrt{x/N^{2p} + r_N^p(\phi_+) + r_N^p(\phi_-)}} - \frac{1}{\sqrt{x/N^{2p}}} &\approx \frac{1}{\sqrt{x/N^{2p}}} \left(1 - \frac{N^{2p}}{2x} (r_N^p(\phi_+) + r_N^p(\phi_-)) - 1 \right) = \\ &= -\frac{1}{2} \left(\frac{N^{2p}}{x} \right)^{3/2} (r_N^p(\phi_+) + r_N^p(\phi_-)). \end{aligned} \quad (51)$$

Because $\int \rho_0(\phi_+)d\phi_+\rho_0(\phi_-)d\phi_-(r_N^p(\phi_+) + r_N^p(\phi_-))$ remains finite, we can neglect the above difference in $f_p(x)$ for small values of p . Hence, we have finally shown that

$$f(N^2x) = \sum_{p=0,1}^{\infty} f_p(N^2x) \approx \sum_{p=0,1}^{\infty} f_{p-1}(x) \approx \sum_{p=0,1}^{\infty} f_p(x) = f(x). \quad (52)$$

We have shown that this equation holds for values x with $ax \ll 1$. Note that even though it is obvious from Figs. 4 and 17 that at about $ax \approx 1$ the pattern is still periodic, we cannot prove this by using the analytical formula (43), which is a perturbative result valid close to the upper border of the interval. Also, the approximation we did in Eq. (48) no longer holds. However, if a is small enough, then the region in question constitutes only a small fraction of the entire repetitive pattern.

6.3 Scaling of expectation values in a

Let us now prove the scaling behaviour of

$$\langle V(\phi) \rangle_a - \langle V(\phi) \rangle_0 = \int_{-1}^1 (\rho_a(\phi) - \rho_0(\phi)) V(\phi) d\phi, \quad (53)$$

where V is a generic test function of the local iterates of the CML. In order to apply the two scaling relations of the previous subsections, we split the integral over ϕ into two parts by choosing a subdivision point $\phi = 1 - ca$. c is arbitrary but fixed (for $N = 2$ e.g. $c = 2^7 = 128$). We obtain $\langle V(\phi) \rangle_a - \langle V(\phi) \rangle_0 = I_u(c) + I_l(c)$ where

$$I_u(c) = \int_{1-ca}^1 (\rho_a(\phi) - \rho_0(\phi)) V(\phi) d\phi, \quad (54)$$

$$I_l(c) = \int_{-1}^{1-ca} (\rho_a(\phi) - \rho_0(\phi)) V(\phi) d\phi. \quad (55)$$

The fact that the integral $I_u(c)$ scales with \sqrt{a} can be shown very easily. From Eq. (44) we obtain

$$\begin{aligned} I_u(c) &= a \int_0^c (\rho_a(1-ax) - \rho_0(1-ax)) V(1-ax) dx \\ &\approx a \int_0^c \left(\frac{1}{\sqrt{a}} g(x) - \frac{1}{\pi\sqrt{2ax}} \right) V(1-ax) dx \approx \sqrt{a} V(1) \int_0^c \left(g(x) - \frac{1}{\pi\sqrt{2x}} \right) dx \end{aligned} \quad (56)$$

where the approximations hold for $ax \ll 1$. If we replace a by λa where λ is (so far) an arbitrary factor and c is kept constant, we obtain

$$I_u(c) \rightarrow \sqrt{\lambda a} V(1) \int_0^c \left(g(x) - \frac{1}{\pi\sqrt{2x}} \right) dx = \sqrt{\lambda} I_u(c). \quad (57)$$

For the second integral $I_l(c)$ we can assume that ϕ is large enough to guarantee the preservation of the pattern given by Eq. (52). We use Eq. (47) to obtain

$$I_l(c) = \sqrt{a} \int_{-1}^{1-ca} f^* \left(-\log_{N^2} \left(\frac{1-\phi}{a} \right) \right) \tilde{V}(\phi) d\phi, \quad \tilde{V}(\phi) = \frac{2\pi V(\phi)}{N\sqrt{2}(1-\phi^2)}. \quad (58)$$

In replacing a by λa we obtain

$$I_l(c) \rightarrow \sqrt{\lambda a} \int_{-1}^{1-\lambda ac} f^* \left(-\log_{N^2} \left(\frac{1-\phi}{a} \right) + \log_{N^2}(\lambda) \right) \tilde{V}(\phi) d\phi. \quad (59)$$

In general, we do not have $I_l(c) \rightarrow \sqrt{\lambda} I_l(c)$ as in the case of the integral $I_u(c)$. However, if we chose $\lambda = 1/N^2$, we can use that $f^*(x^*)$ is (nearly) periodic with period 1 to obtain

$$I_l(c) \rightarrow \frac{1}{N} \sqrt{a} \int_{-1}^{1-ac/N^2} f^* \left(-\log_{N^2} \left(\frac{1-\phi}{a} \right) \right) \tilde{V}(\phi) d\phi = \frac{1}{N} I_l(c/N^2). \quad (60)$$

If we replace the upper limit of the integral by $1 - ca$, we neglect an integration range in ϕ of length of order $O(a)$. Therefore, in leading order we obtain $I_l(c) \rightarrow I_l(c)/N$. Collecting both results, we finally obtain that under the transformation $a \rightarrow a/N^2$ we have

$$\langle V(\phi) \rangle_a - \langle V(\phi) \rangle_0 \rightarrow \langle V(\phi) \rangle_{a/N^2} - \langle V(\phi) \rangle_0 = \frac{1}{N} (\langle V(\phi) \rangle_a - \langle V(\phi) \rangle_0) \quad (61)$$

whereas for general transformations $a \rightarrow \lambda a$ we obtain a result different from a simple multiplication by a factor $\sqrt{\lambda}$. It is obvious, then, that we have

$$\langle V(\phi) \rangle_a - \langle V(\phi) \rangle_0 = \sqrt{a} f_N^V(\log_{N^2}(a)) \quad (62)$$

where $f_N^V(\log_{N^2}(a))$ is a periodic function with period 1 depending on the test function $V(\phi)$.

Conclusion

The treatment of nonhyperbolic CMLs exhibiting chaotic behaviour is notoriously more difficult than that of hyperbolic ones. In this paper we tackled the problem by introducing an iterative convolution technique that provides a perturbative expression for invariant 1-point and 2-point densities. For small coupling parameters a the invariant 1-point density ρ_a of the CML is obtained as a sum of density contributions $\rho_a^{(p)}$, where the index p essentially describes at which time in the past the nonhyperbolic region is active in our convolution scheme. We obtained explicit perturbative expressions for the densities of diffusively coupled Tchebyscheff maps of N -th order. Our main examples were the cases $N = 2$ and $N = 3$, which significantly differ in their symmetry properties. While in the uncoupled case the invariant 1-point density is smooth, an arbitrarily small coupling a induces a selfsimilar cascade of patterns with a variety of cusps and non-differentiable points, which can all be understood by our perturbative approach. We proved that arbitrary expectation values scale with the square root of the coupling parameter and that there are log-periodic oscillations both in the phase space and in the parameter space. Though, for reasons of concreteness, we mainly dealt with 2nd and 3rd order Tchebyscheff maps, our techniques can be applied in a similar way to other nonhyperbolic coupled systems where the local maps exhibit fully developed chaos.

Acknowledgements

This work is supported in part by the Estonian target financed project No. 0182647s04 and by the Estonian Science Foundation under grant No. 6216. S. Groote acknowledges support from

a grant given by the Deutsche Forschungsgemeinschaft for staying at Mainz University as guest scientist for a couple of months. C. Beck's research is supported by a Springboard Fellowship of the Engineering and Physical Sciences Research Council (EPSRC).

References

- [1] K. Kaneko, *Progr. Theor. Phys.* **72**, 480 (1984)
- [2] R. Kapral, *Phys. Rev. A* **31**, 3868 (1985)
- [3] K. Kaneko (ed.), *Theory and Applications of Coupled Map Lattices*, John Wiley and Sons, New York (1993)
- [4] C. Beck, *Spatio-temporal chaos and vacuum fluctuations of quantized fields*, World Scientific, Singapore (2002)
- [5] A. Bunimovich, Ya.G. Sinai, *Nonlinearity* **1**, 491 (1988)
- [6] R.E. Amritkar and P.M. Gade, *Phys. Rev. Lett.* **70**, 3408 (1993)
- [7] R. Carretero-Gonzales, D.K. Arrowsmith and F. Vivaldi, *Physica D* **103**, 381 (1997)
- [8] L.A. Bunimovich, *Physica D* **103**, 1 (1997)
- [9] V. Baladi and H.H. Rugh, *Comm. Math. Phys.* **220**, 561 (2001)
- [10] J. Bricmont, A. Kupiainen, *Comm. Math. Phys.* **178**, 703 (1996)
- [11] E. Järvenpää and M. Järvenpää, *Comm. Math. Phys.* **220**, 1 (2001)
- [12] H. Daido, *Progr. Theor. Phys. Suppl.* **79**, 75 (1984)
- [13] A. Lemaître and H. Chaté, *Europhys. Lett.* **39**, 377 (1997)
- [14] W. Yang, E-Jiang Ding and M. Ding, *Phys. Rev. Lett.* **76**, 1808 (1996)
- [15] A. Torcini, R. Livi, A. Politi and S. Ruffo, *Phys. Rev. Lett.* **78**, 1391 (1997)
- [16] M.C. Mackey and J. Milton, *Physica D* **80**, 1 (1995)
- [17] C. Beck, *Physica D* **171**, 72 (2002)
- [18] C. Beck, *Nonlinearity* **8**, 423 (1995)
- [19] C. Beck, *Phys. Rev. D* **69**, 123515 (2004)
- [20] C.P. Dettmann, *Physica D* **172**, 88 (2002)
- [21] C.P. Dettmann and D. Lippolis, *Chaos Sol. Fractals* **23**, 43 (2005)
- [22] S. Groote and C. Beck, [nlin.CD/0603397](https://arxiv.org/abs/nlin.CD/0603397)

- [23] C. Beck, F. Schlögl, *Thermodynamics of Chaotic Systems*, Cambridge University Press, Cambridge 1993
- [24] V. Baladi, *Positive Transfer Operators and Decay of Correlations*, World Scientific, Singapore 2000
- [25] G. Keller and M. Künzle, *Erg. Th. Dyn. Syst.* **12**, 297 (1992)
- [26] A. Lemaître, H. Chaté and P. Manneville, *Europhys. Lett.* **39**, 377 (1997)
- [27] H. Chaté and J. Losson, *Physica D* **103**, 51 (1997)
- [28] C. Tsallis, *J. Stat. Phys.* **52**, 479 (1988)